The role of white matter myelin in structural-functional network coupling

Short title: White matter myelin supports functional connectivity

Mark C. Nelson[1,2], Wen Da Lu[2,3], Ilana R. Leppert[2], Heather A. Hansen[1], Christopher D. Rowley[4], Bratislav Misic[1,2], and Christine L. Tardif [1,2,3]

[1]*Department of Neurology and Neurosurgery, McGill university, Montreal, QC, Canada.* [2]*McConnell Brain Imaging Centre, Montreal Neurological Institute and Hospital, Montreal, QC, Canada.* [3]*Department of Biomedical Engineering, McGill University, Montreal, QC, Canada.* [4]*Department of Physics and Astronomy, McMaster University, Hamilton, ON, Canada.*

Corresponding Author: Christine Tardif, christine.tardif@mcgill.ca

Abstract

The brain is a complex network of neuronal populations interconnected by white matter tracts. The composition of these white matter connections (SC) shapes inter-regional signaling dynamics giving rise to spatial patterns of synchronous functional connectivity (FC). Several modeling approaches have proven useful for studying the mechanisms underlying the relationship between SC and FC. However, the myelination of white matter tracts — a major component of white matter connectivity — is not accounted for by conventional SC networks, and thus, has largely been excluded from models of FC. Here, we expand structure-function brain modeling by integrating a multi-feature white matter SC network. We use multi-modal MRI to compute an SC network with connections (edges) weighted by the caliber, myelination, and length of white matter tracts. We investigate the relationship of this multi-feature SC

network with both haemodynamic and electromagnetic FC. Edge myelin was strongly predictive of FC in a pattern that was heterogeneous across brain regions and timescales of neural function. Edge myelin showed strong, frequency-specific interactions with both edge caliber and length suggesting a modulatory role for white matter myelin in structure-function coupling. This was further supported by antagonistic gradients of white matter myelin and structure-function coupling along the sensory-association axis. We describe in detail the individual and joint relationships between these major white matter features and multi-frequency FC. These results illustrate the advantage of a more comprehensive characterization of white matter in structure-function models and establish how white matter myelin — known for roles in conduction velocity, plasticity, and metabolic support at the microscale — shapes brain function at the macroscale.

Introduction

Be it an ecosystem, an economy, or an encephalon, the form and function of complex systems are intricately linked(M. E. J. Newman, 2003). By applying the principles of network science(M. Newman, 2010) to the human brain(Bassett & Sporns, 2017; Fornito et al., 2016; Sporns, 2010; Suárez et al., 2020), a modular and small-world architecture is revealed which facilitates both specialized processing within regions, as well as efficient global communication. A fundamental component of this relationship is the arrangement and properties of the physical connections (edges) between regions (nodes), which constrain and shape the landscape of dynamic functional interactions(Sporns, 2011). The characterization of the mechanisms through which brain structure and function interact is a central goal in neuroscience.

Through the non-invasive lens of multi-modal magnetic resonance imaging (MRI), networks of macroscale connectivity between nodes can be estimated in the human brain *in vivo*. Functional connectivity (FC)(Salvador et al., 2005) typically quantifies the cross-correlation of blood-oxygen-level dependent (BOLD) functional MRI (fMRI) time series(Biswal et al., 1995), and structural connectivity (SC)(Hagmann et al., 2008; Honey et al., 2009) reconstructs the interconnecting white matter pathways by combining diffusion-weighted MRI with streamline tractography(Basser et al., 1994; Mori & Barker, 1999; Mori & Van Zijl, 2002). At this scale, network nodes amount to volumes of roughly 10^2-10^4 mm^3 containing as many as 10^8 neurons(Azevedo et al., 2009; Goriely, 2025), and structural edges likely represent the aggregate of both mono- and poly-synaptic white matter fiber pathways between these large gray matter regions.

While this spatial resolution may seem quite coarse, multiple modeling approaches have consistently demonstrated that SC based on diffusion MRI is predictive of BOLD-FC(Seguin et al., 2023; Suárez et al., 2020), and the link between them has implications for human behavior(Preti & Van De Ville, 2019; Seguin et al., 2020) and cognition(Litwińczuk et al., 2022; Popp et al., 2024; Shine et al., 2019). A spatially heterogeneous pattern of structural-functional network coupling has emerged(Liu et al., 2023; Preti & Van De Ville, 2019; Vázquez-Rodríguez et al., 2019; Zamani Esfahlani et al., 2022), which is closely aligned with the primary axis of cortical organization: the sensory-association (S-A) axis(Huntenburg et al., 2018; Sydnor et al., 2021). This places structure-function coupling alongside other large-scale features such as cortical hierarchy(Margulies et al., 2016; Mesulam, 1998), as well as finer-grained cortical features, including laminar differentiation(Paquola et al., 2019), intracortical myelin(Glasser &

Van Essen, 2011; Huntenburg et al., 2017), neurotransmitter receptor distributions(Hansen et al., 2022) and gene expression(Burt et al., 2018).

Macroscale FC networks can also be derived from time series recorded with magnetoencephalography (MEG), which facilitates the assessment of neural function at higher frequencies (1-100+Hz) than BOLD-fMRI (0.01-0.5Hz). The fMRI signal is thought to reflect a superposition of these neurophysiological rhythms(Shafiei et al., 2022) and their cross-frequency interactions(Tewarie et al., 2016). Cross-frequency coupling plays an important role in the formation of brain networks both during rest(Florin & Baillet, 2015; Tewarie et al., 2016) and task(Brookes et al., 2016). Higher frequencies tend to reflect bottom-up sensory processing and lower frequencies top-down modulation(Baillet, 2017; Fries, 2015; Hillebrand et al., 2016; Scheeringa & Fries, 2019; Von Stein et al., 2000), which manifests as a gradient of timescales of neural function(Chaudhuri et al., 2015; Mahjoory et al., 2020; Murray et al., 2014) aligned with the S-A axis. Although these relationships — as with BOLD-fMRI — have been linked to multi-scale cortical structure(Helbling et al., 2015; Hunt et al., 2016; Mahjoory et al., 2020; Scheeringa & Fries, 2019) and conventional SC(Garcés et al., 2016), much less is known about the coupling between white matter structural and MEG-functional networks.

Thus, we come to a principal limitation of structure-function modeling: current models lack the requisite biological detail to draw strong conclusions about the underlying mechanisms(Suárez et al., 2020). One way to address this at the whole-brain level *in vivo* is by weighting the edges of structural networks using MRI-derived measures of white matter structure relevant to brain function(Assaf et al., 2008; Boshkovski et al., 2021; Caeyenberghs et al., 2016; Deligianni et al., 2016; Gast & Assaf, 2024; Lu et al., 2025; Mancini et al., 2018; Messaritaki et al., 2021; Nelson et al., 2023; Stikov et al., 2015; M. P. van den Heuvel et al., 2010). In

92 particular, MRI-based estimates of white matter myelin density have been linked to both brain
93 organization and function(Sonya Bells et al., 2017; Caeyenberghs et al., 2016; Gong et al., 2024;
94 Messaritaki et al., 2021; Nelson et al., 2023; Petkoski et al., 2023).

95 The myelination of axonal fibers helps to regulate the timing of neural signaling(Huxley
96 & Stämpfli, 1949; Lillie, 1925; Tasaki, 1939) supporting synchronization across distributed
97 neural circuits(Nunez et al., 2015; Nunez & Srinivasan, 2014; Pajevic et al., 2014). Conversely,
98 the plastic structure of myelin is itself shaped by neuronal activity, thus establishing a reciprocal
99 mechanistic link between the modulation of white matter myelin and inter-regional functional
100 coherence(Bacmeister et al., 2022; Chorghay et al., 2018; Douglas Fields, 2015; Fields et al.,
101 2015; Mount & Monje, 2017; Zatorre et al., 2012). Although its role in conduction velocity is
102 less clear at the macroscale(Berman et al., 2019; Mancini et al., 2021; Petkoski et al., 2023;
103 Talidou & Lefebvre, 2025), white matter myelin is believed to support brain function through
104 varied contributions including: gain control, circuit integration, resilience, and
105 homeostasis(Karimian et al., 2019; Noori et al., 2020; Park & Lefebvre, 2020), as well as
106 metabolism(Asadollahi et al., 2024; Nave, 2010; Ramos-Cabrer et al., 2025), and
107 energetics(Harris & Attwell, 2012).

108 Myelination patterns in both the white matter and cortex are linked to the major S-A axis
109 of brain organization. Along this gradient, intracortical myelin content decreases(Glasser et al.,
110 2014; Glasser & Van Essen, 2011), and white matter tracts are myelinated progressively
111 later(Fuster, 1995, 2008): primary sensory regions with high intracortical myelin myelinate their
112 axons first. There is also evidence of both axis-general and axis-specific patterns of development
113 for the strength of white-matter connectivity. Within-network connections at both ends of the
114 axis become stronger over development, increasing network modularity and sharpening the

differentiation of cortico-cortical systems. At the same time, inter-modular integration increases—but this occurs selectively through the strengthening of long-range association-hub connections, rather than uniformly across the axis(Sydnor et al., 2021). This topological pattern – – also supported by MRI-based metrics of white matter myelin(Boshkovski et al., 2021) — is fundamental to the brain structure-function relationship(Sporns, 2010, 2011, 2013). Thus, a coordinated blueprint of cerebral myelination gives rise to a global axis of myelin content, which is linked to the organization of both brain structure and function.

Despite these links to brain function, white matter myelin has largely been excluded from structure-function models. How does white matter myelin relate to global FC, and does this relationship vary across brain regions and functional timescales? Here, we address these questions by integrating white matter tract features including myelin into a network model of FC. Specifically, we combine a network analysis approach with multi-modal MRI to quantify three major features of white matter connectivity at the network edge level: caliber, myelin, and length. We then use these features in an edge-wise multi-linear model to predict haemodynamic and electromagnetic FC. Based on previous work(Nelson et al., 2023), we expect that myelin and BOLD-FC will be inversely related globally. We further hypothesize that the regional coupling of myelin and BOLD-FC will be stronger, heterogeneous, and aligned with the S-A axis, in line with results using spectral(Preti & Van De Ville, 2019) and communication features(Liu et al., 2023; Vázquez-Rodríguez et al., 2019; Zamani Esfahlani et al., 2022) from conventional SC. Anticipating the coupling between myelin and MEG-FC is challenging, as few or no studies have explored this. However, it is reasonable to expect stronger, heterogeneous, and frequency-specific coupling regionally, as shown for conventional SC(Liu et al., 2023).

Results

Multi-modal MRI data acquired at 3 tesla in 30 healthy adults (14 men, 16 women; 29±6 years of age) were used to estimate the SC and in-sample FC networks. Structural connections were derived by applying streamline tractography to diffusion MRI data, then weighted by edge-level estimates of the caliber, myelin, and length of white matter tracts. Edge caliber quantifies the total cross-sectional area of the intra-axonal compartment. Edge myelin quantifies myelin density and was derived from tractometry of magnetization transfer saturation images. The in-sample FC network was estimated as the zero-lag Pearson cross-correlation of node-wise time series from resting-state (task-free) BOLD-fMRI data (**$BOLD_{in}$**). Group-averaging resulted in four connectivity networks (caliber, myelin, length, and $BOLD_{in}$) from in-sample data. An additional seven out-of-sample FC networks were obtained in fully preprocessed(Shafiei et al., 2022) and group-averaged format: one from resting-state fMRI (**$BOLD_{out}$**) and six from resting-state MEG corresponding to the canonical electrophysiological frequency bands: **delta** (2-4Hz), **theta** (5-7Hz), **alpha** (8-12Hz), **beta** (15-29Hz), **$gamma_{lo}$** (30-59Hz), and **$gamma_{hi}$** (60-90Hz). These were derived from data in healthy participants (n = 33; age range 22 to 35 years) made openly available through the Human Connectome Project (HCP; S900 release(Van Essen et al., 2013)). Thus, eight unique FC networks were separately modeled as linear combinations of three weighted SC networks including interaction terms for both caliber and length with myelin (**Figure 1a**). Modeling was performed at three spatial scales: global (whole-brain), pairwise combinations of resting-state networks, and at the level of individual nodes. Network nodes were defined using the Schaefer-400(Schaefer et al., 2018) cortical atlas. The correlation between all structural features and all FC networks is shown in **Figure S9**

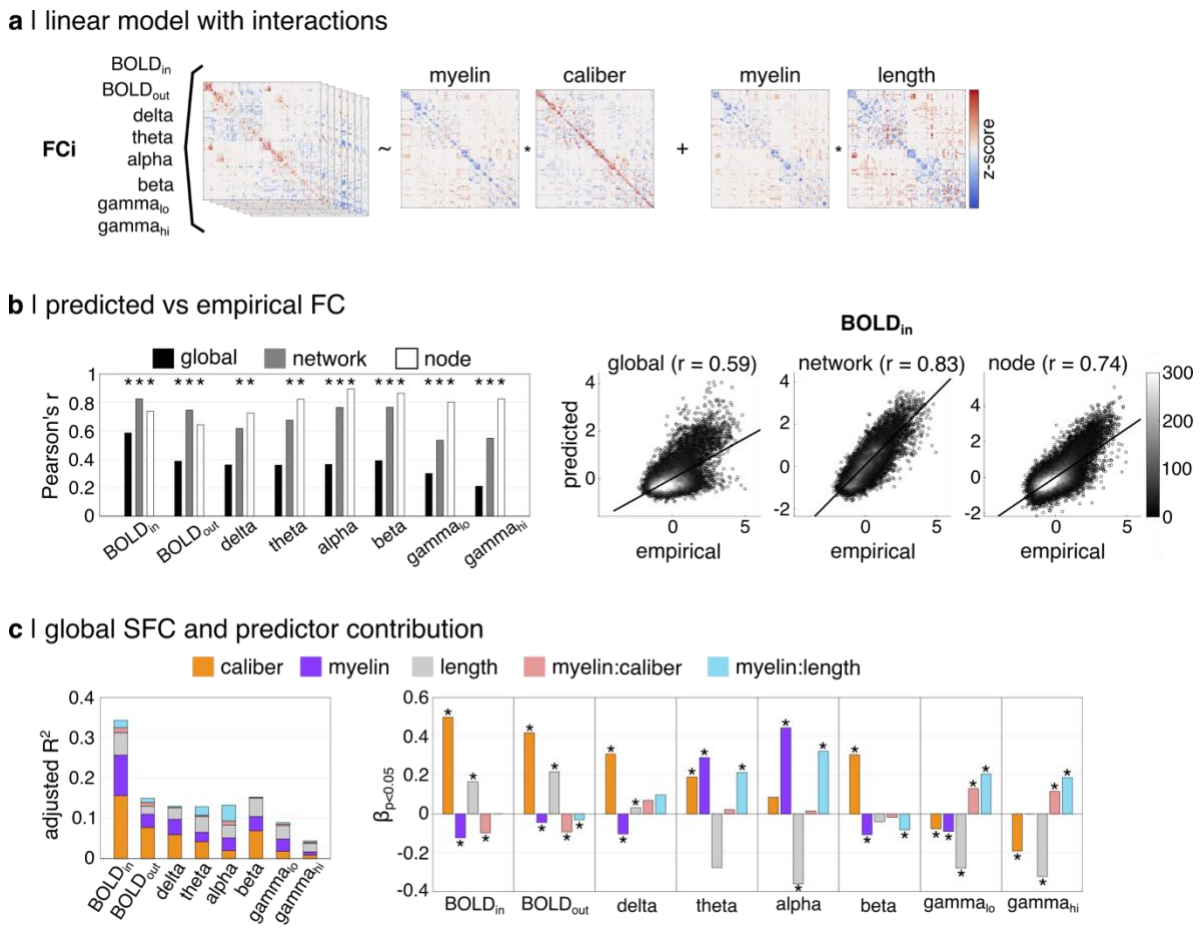

Figure 1. Relating white matter structural features to haemodynamic and electromagnetic functional connectivity. ***(a)*** *An edgewise multi-linear regression model predicting FC from SC. FC was quantified using BOLD-fMRI and multi-band MEG. SC was quantified as the caliber, myelin and length of white matter tracts from multi-modal MRI. Interaction terms with myelin were included for caliber and length. All data was z-scored before modeling.* ***(b)*** *Pearson's correlations of predicted vs empirical FC at global, network and node-level resolutions. Edges were pooled for correlations at network and node-levels. All correlations were significant ($p_{perm} < 0.05$), except global delta and theta. Scatter plots (right) are shown for $BOLD_{in}$.* ***(c)*** *Global SFC strength (left) is quantified using adjusted R^2. Colored bar segments show ratio of predictor contributions from dominance analysis. Standardized ß-coefficients (right) surviving parametric t-tests ($p < 0.05$) are shown. Asterisks additionally indicate significance from permutation testing ($p_{perm} < 0.05$) and $0 \notin 95\%$ confidence intervals.*

White matter myelin supports haemodynamic and electromagnetic connectivity

FC values predicted by the model correlated strongly with empirical FC data (**Figure 1b**). The correlation magnitude increased with model resolution for both MEG and fMRI, however the optimal resolution was modality-dependent and mirrored their temporal resolution differences:

strongest at the network level for BOLD ($r > 0.75$, $p_{perm} = 0.001$) and at the node level for MEG ($r > 0.70$, $p_{perm} = 0.001$). Node-level alpha and beta models showed the highest correlations ($r > 0.85$, $p_{perm} = 0.001$). Delta and theta models failed to reach significance at the global level when applying a spatially-constrained permutation test.

We assessed the global relationship between white matter edge features and FC by pooling all upper triangle edges with $SC \neq 0$ into a single model (**Figure 1c**). The strength of structure-function coupling (SFC) was inferred from model fit (adjusted coefficient of determination; R^2). The contribution of each structural feature to the prediction of FC was quantified in two ways: (1) their relative importance from *dominance* analysis(Azen & Budescu, 2003; Budescu, 1993), and (2) the nature of their *association* from the sign and magnitude of standardized ß coefficients.

SFC was strongest for $BOLD_{in}$ ($R^2 = 0.34$), lowest for the gamma bands ($R^2 < 0.09$), and roughly equivalent for $BOLD_{out}$ and delta-beta ($R^2 \sim 0.13$-0.15). Myelin was a strong predictor of FC in both BOLD and MEG data. Myelin ranked 2nd in predictor dominance behind caliber for $BOLD_{in/out}$ and delta, dropped to 3rd for theta and beta as the relative importance of length increased in MEG, and shared dominance with length for alpha and gamma as caliber decreased in importance at higher frequencies. The ß-coefficients for all predictors showed frequency-dependent sign and magnitude, and nearly all were significant ($p_{perm} < 0.05$ and parametric $p < 0.05$). All predictors failing to reach significance were observed for MEG-FC models including: myelin for $gamma_{hi}$, caliber for alpha, and length for theta and beta. $ß_{myelin}$ was negative for BOLD, delta, beta and $gamma_{lo}$, in line with the global correlation of myelin and BOLD-FC(Nelson et al., 2023). $ß_{myelin}$ was positive and higher in magnitude for theta and alpha. A

200 similar sign flip was observed for caliber (ß > 0 for BOLD and most MEG bands; ß < 0 for
201 gamma) and length (ß > 0 for BOLD and ß < 0 for most MEG bands).
202 The interaction terms tended to be the lowest ranked predictors across models, reflecting
203 their general role of fine tuning the larger effects of their respective lower order terms.
204 Nonetheless, most interaction terms were significant and showed heterogeneous sign and
205 magnitude across FC modality and frequency. Interestingly, the interaction term between myelin
206 and length ranked 1st in predictor dominance for alpha-band MEG and showed a large magnitude
207 positive ß-weight indicating that the role of myelin is strengthened for longer edges. We expand
208 on these interactions with myelin in subsequent sections.
209 These results communicate two important points about the structure-function relationship
210 of the brain. First, white matter myelin is an important predictor of whole-brain FC showing
211 comparable predictive power to the much more extensively studied white matter edge features
212 caliber and length. Second, the specific roles of white matter features including myelin in
213 mediating brain function depend on the cellular processes contributing to the measurement
214 technique (haemodynamic vs electromagnetic) and the timescale of the signal (frequency bands).
215

216 ***Haemodynamic and electromagnetic connectivity show distinct, spatially varying***
217 ***relationships with white matter myelin***

218 Several reports have demonstrated regional heterogeneity in SFC using conventional SC directly
219 or analytic measures derived therefrom(Baum et al., 2020; Liu et al., 2023; Preti & Van De Ville,
220 2019; Vázquez-Rodríguez et al., 2019; Zamani Esfahlani et al., 2022). Given our observations
221 above and the diversity of mechanisms by which myelin supports brain function, we next sought
222 to describe how the coupling of edge myelin and FC varies across brain regions. We ran the

same multi-linear model at two additional spatial scales: (1) within pairwise combinations of the seven canonical resting-state networks(Thomas Yeo et al., 2011), and (2) within the connections of each individual node i to the remaining $j \neq i$ nodes. The limbic-somatomotor network pair was excluded for low degrees of freedom (d.f. < 10). We observed high correspondence between the network (**Figure 2**, **4**, **S1**, and **S2**) and node (**Figure 3** and **S3**-**S5**) levels. We thus focus this description on results from the network-level models as they are more robust (μ d.f. ≈ 875 vs 85) and efficient (n = 28 models vs 400).

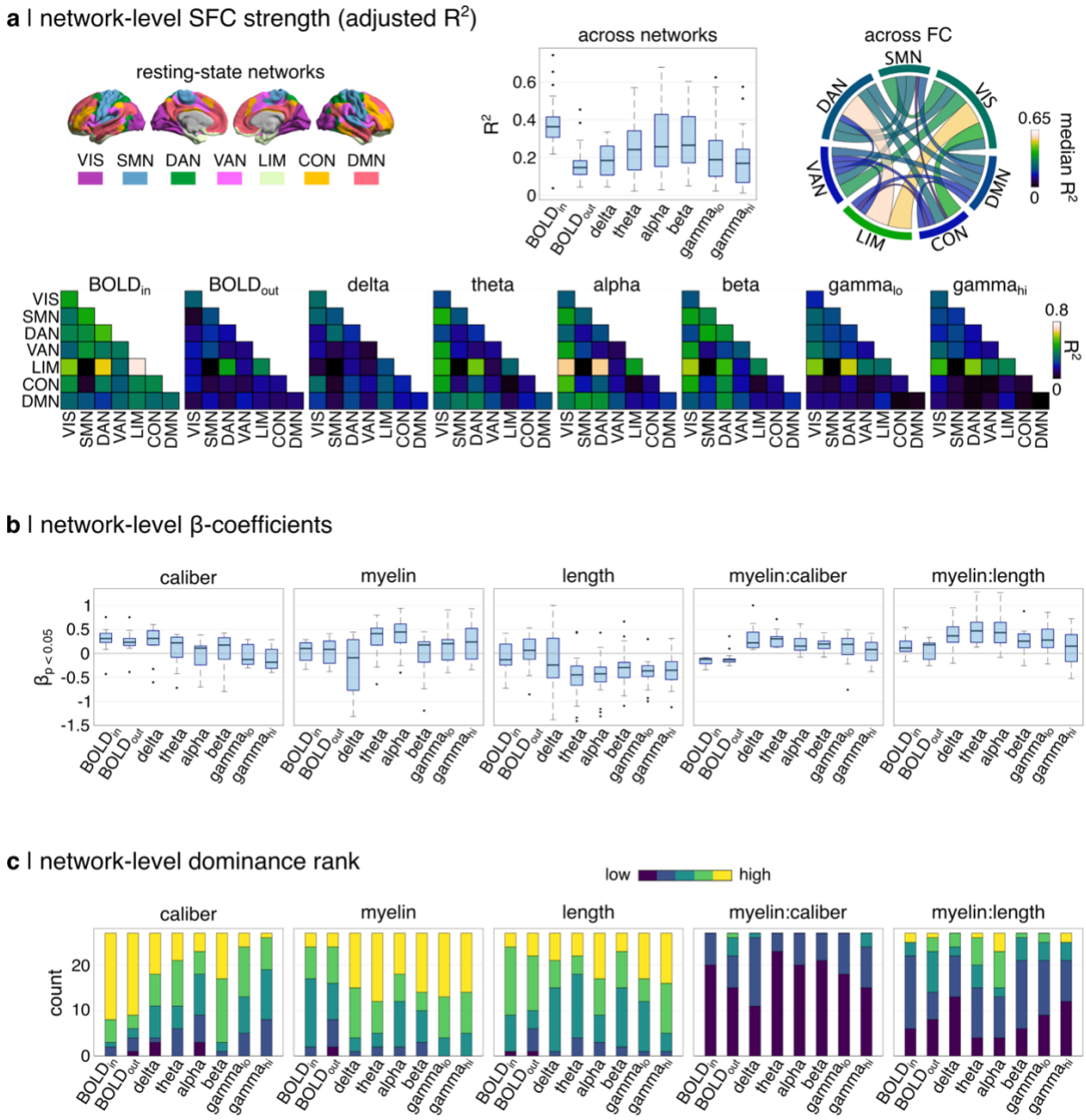

Figure 2. Relating white matter structural features to haemodynamic and electromagnetic connectivity at the level of pairwise combinations of resting-state networks. ***(a)*** *SFC strength for pairwise combinations of resting-state networks defined using the Yeo 7-network atlas (top left). Boxplots (top middle) show the distribution of SFC across network pairs using standard elements: median line, 1st and 3rd quartile box limits, 1.5 interquartile range whiskers, and outlier data points. The circle plot (top right) shows the median value across FC networks with the network bars along the perimeter indicating the within-network values. SFC for every network pair and FC network is also shown in matrix form (bottom).* ***(b)*** *The distribution of standardized ß-coefficients and* ***(c)*** *the count of dominance rankings is shown for all predictors.*

Across network pairs and FC timescales, there was considerable heterogeneity in SFC (**Figure 2a**), as well as in the standardized ß-coefficients (**Figure 2b** and **4**) and predictor

243 dominance rankings (**Figure 2c** and **S1**) for caliber, myelin, length, and both myelin interaction
244 terms. SFC was strongest for $BOLD_{in}$ followed by alpha and beta. Network pairings involving
245 primary sensory regions (visual and somatomotor) showed stronger SFC than those involving
246 association regions (default mode, control, and attentional). The strongest SFC was observed for
247 the limbic-dorsal attention, limbic-visual, and limbic-limbic network pairs. At the node-level,
248 SFC showed significant inverse correlations with the sensory-association axis for all FC
249 networks, except alpha (**Figure 3c**). $BOLD_{in}$ showed the most spatially distributed pattern of
250 strong SFC, with the highest values spread across central, parietal, temporal, and occipital
251 cortical regions (**Figure 3b** and **S3**).
252

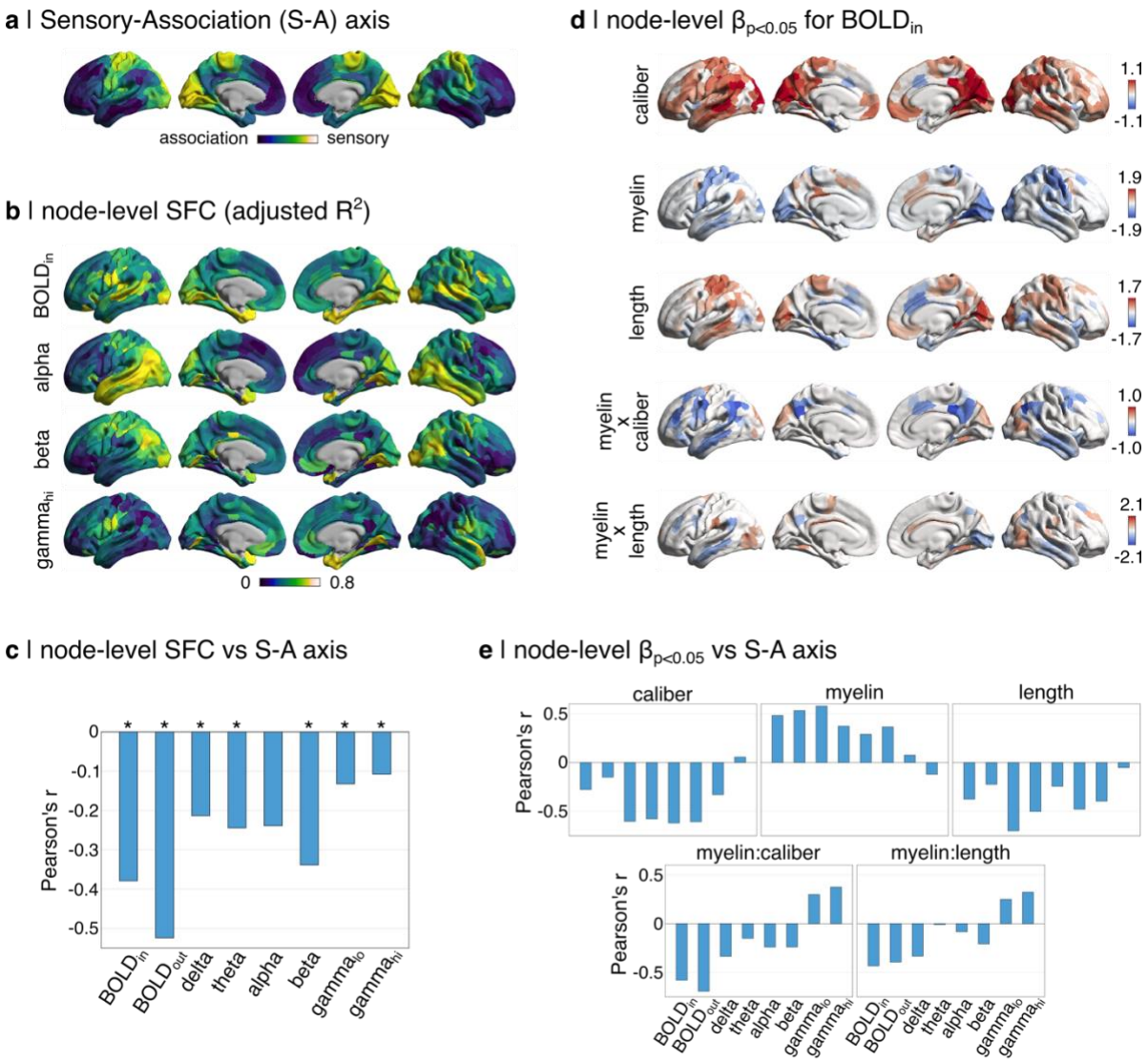

Figure 3. Alignment of node-level model coefficients with the sensory-association (S-A) axis. ***(a)*** *The S-A axis is shown in the Schaefer-400 parcellation. Node values are shown for* ***(b)*** *SFC for several FC models, as well as the* ***(d)*** *ß-coefficients from the* $BOLD_{in}$ *model for all structural predictors. Pearson's correlation was used to quantify alignment for* ***(c)*** *SFC and* ***(e)*** *ß-coefficients for all predictors and FC models. All ß-values were filtered by parametric t-tests (p < 0.05). Asterisks additionally indicate significance from spatially-constrained permutation testing (*p_{perm} *< 0.05).*

The standardized ß-coefficients for caliber, myelin, and length (**Figure 2b** and **4**) showed both positive and negative values across network pairs and an interesting frequency dependence. $ß_{caliber}$ showed a gradual transition from mostly positive to negative values when moving from low-to-high frequency FC (including BOLD), while $ß_{myelin}$ showed an opposite trend: balanced

for BOLD and delta, and more positive for theta through gamma. $ß_{length}$ showed predominantly negative values, with exceptions for BOLD-FC and unimodal networks for most models.

Among network pairs, the spatial pattern of positive and negative $ß_{myelin}$ was on average inversely aligned with the canonical unimodal-transmodal gradient of cortical organization: positive for network pairs involving transmodal association networks and negative for unimodal (**Figure S2a**). In contrast, $ß_{caliber}$ was on average positive within a given network and mixed between networks regardless of their position on the gradient. Interestingly, the ß-coefficients for both myelin and caliber deviated from these average trends for gamma: $ß_{myelin}$ was mostly positive including for unimodal networks, and $ß_{caliber}$ was mostly negative including within-network (**Figure 4a** and **4b**). The ß-coefficients for both interaction terms were significant across most network pairs (**Figure 4d** and **4e**). $ß_{myelin:caliber}$ was mostly negative for BOLD and positive for MEG. $ß_{myelin:length}$ was mostly positive and tended to be larger. These interactions are explored in more detail in the subsequent section.

At the node-level, $ß_{caliber}$ and $ß_{length}$ were inversely correlated and $ß_{myelin}$ positively correlated with the S-A axis across FC networks (**Figure 3e**). These trends were weakest or absent in the highest frequency gamma. $ß_{myelin}$ tended to be larger in magnitude than $ß_{caliber}$ (**Figure S5b**).

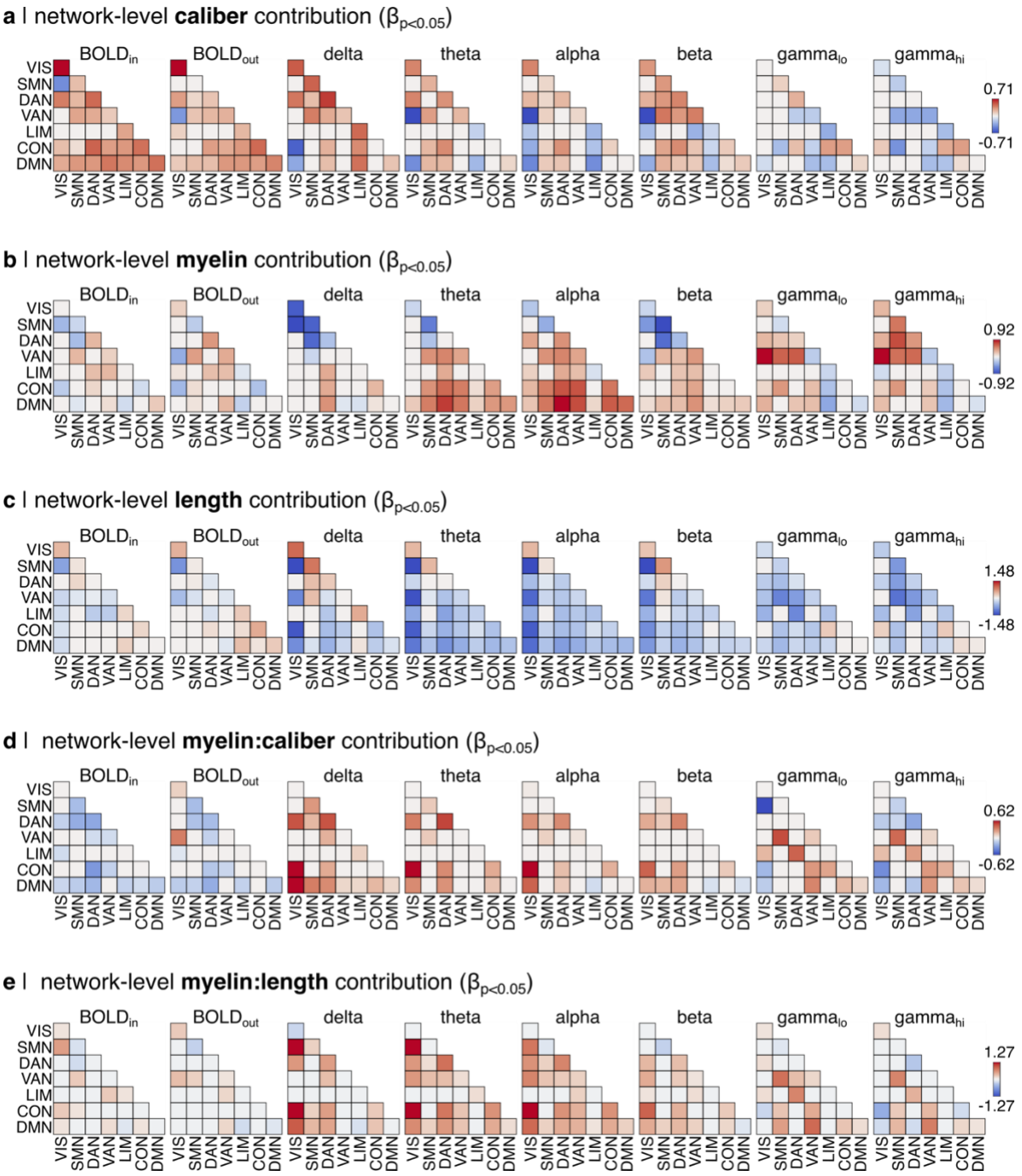

*Figure 4. Standardized ß-coefficients for edge **(a)** caliber, **(b)** myelin, **(c)** length, **(d)** the interaction of myelin and caliber, and **(e)** the interaction of myelin and length at the pairwise network level for all FC models. Only significant values are shown (t-test $p < 0.05$).*

We also observed a frequency-dependence for the network-level predictor dominance rankings of caliber, myelin, length, and both myelin interaction terms (**Figure 2c** and **S1**). Caliber tended to rank 1st and myelin 2nd for BOLD. As FC frequency increased, length became

more dominant and caliber became less dominant, such that myelin and length shared dominance for most network pairs in alpha and gamma. Beta resembled BOLD but with greater influence of length. Myelin showed strong interactions, especially with length for alpha and theta. At the node-level, caliber tended to dominate in frontal and temporal regions and myelin in central, parietal and occipital regions for BOLD (**Figure S4**).

With these results, we have revealed distinct spatial patterns of structure-function coupling for each frequency band. Furthermore, we have demonstrated how these relationships can be decomposed to examine the influence of individual predictors (white matter features). Despite the heterogeneity of spatial patterns, there is generally a shared alignment with the sensory-association axis across predictors and most frequencies of FC.

Antagonistic gradients of structure-function coupling and white matter myelin

Next, we dove deeper into the strong interactions with myelin reported above by asking how the relationships of caliber and length with FC may be different for high vs low myelin edges. We partitioned network edges into 5 equal-sized bins ($n \approx 3667$) according to the magnitude of their myelin weight (**Figure 5a**). Within these bins, we computed Pearson's correlations of the z-scored SC and FC edge weights, as well as a version of the previously described multi-linear model excluding the myelin-interaction terms.

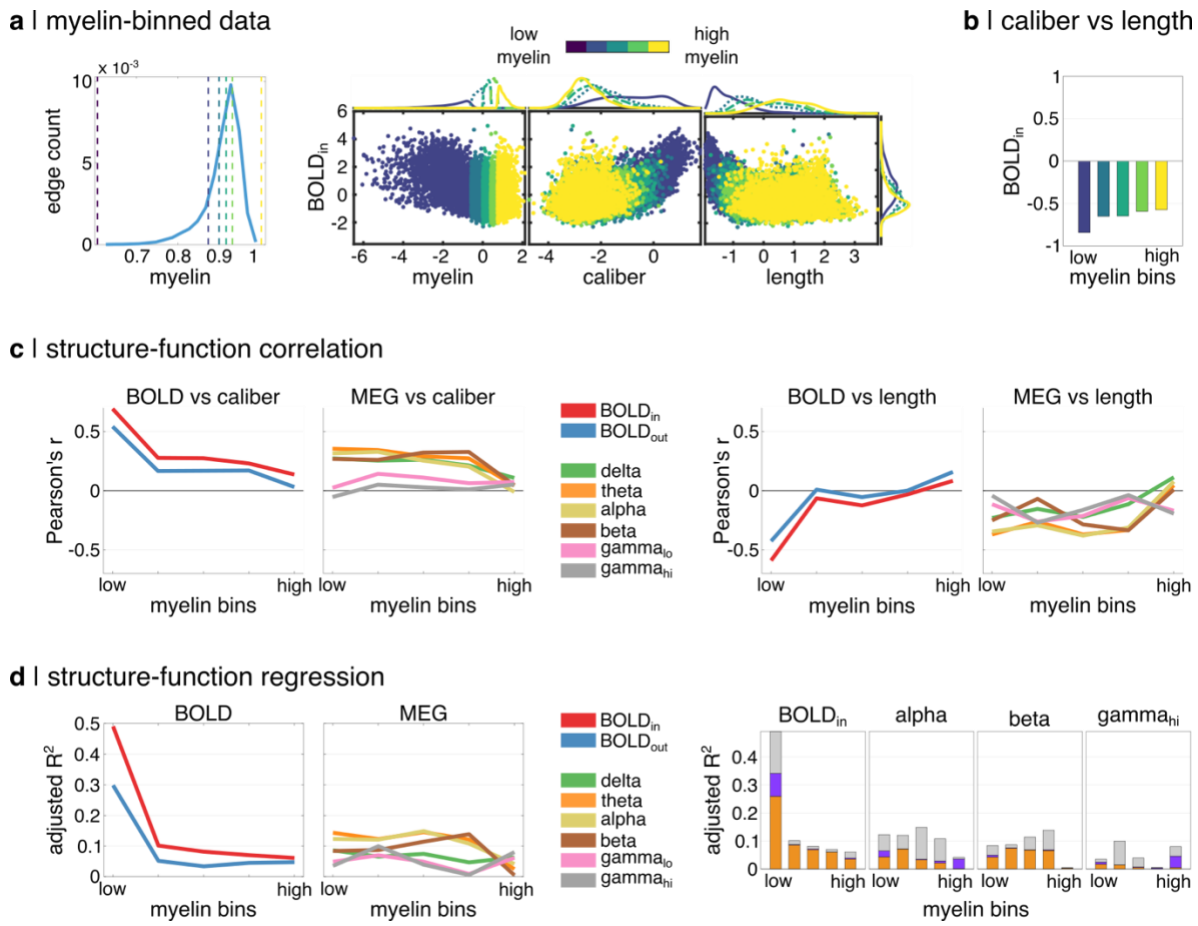

Figure 5. The coupling of white matter structure and FC weakens along the gradient of white matter myelin. ***(a)*** *Network edges were partitioned into 5 equal-sized bins by edge myelin magnitude. Each bin contained 20% or ≈ 3667 network edges.* ***(b)*** *The Pearson correlation of caliber and length across myelin bins.* ***(c)*** *The Pearson correlation of caliber (left) and length (right) with both BOLD-FC and MEG-FC is shown across myelin bins.* ***(d)*** *SFC (adjusted R^2) across myelin bins is shown for all FC networks (left) and for a subset including predictor dominance ratios (right).*

While the relationship between caliber and length remained relatively constant with increasing myelin magnitude (**Figure 5b**), both length and caliber uncoupled from BOLD-FC and low-intermediate frequency MEG-FC (delta, theta, alpha, beta) (**Figure 5c**). This trend is in line with a potential role for white matter myelin in mediating the relationship between FC and white matter edge macrostructure. For BOLD-FC, this uncoupling effect was gradual for caliber, whereas the correlation of length and BOLD-FC was already near 0 in the 2nd myelin bin. For low-to-intermediate frequency MEG, uncoupling of either length or caliber did not occur until the final bin with the highest myelin magnitude. The gamma bands remained relatively

323 uncoupled from caliber independent of myelin and showed distinct patterns of coupling with
324 length.

325 For BOLD, SFC was much stronger when myelin was lowest ($BOLD_{in}$ $R^2 = 0.49$;
326 $BOLD_{out}$ $R^2 = 0.30$) and decreased dramatically with increasing myelin magnitude (**Figure 5d**).
327 The predictor contributions show that this reduction in SFC is driven by a large reduction in the
328 impact of caliber and a complete elimination of length. For theta, alpha, and beta bands, caliber
329 and length continue to drive consistent SFC until a drop off in the final high myelin bin. Delta
330 and gamma deviate from this trend by showing weak relationships with structure in all myelin
331 bins. These results provide evidence for a progressive dissociation of white matter structural and
332 functional connectivity with increasing white matter myelin content. The modality-specificity of
333 this effect highlights the multi-layered relationship between brain structure and function.
334

335 *A multi-feature structural model predicts robust general FC patterns but weak*
336 *subject-specificity*

337 Our final goal was to assess the generalizability of the full linear model with interaction terms to
338 unseen subject-level data from $BOLD_{in}$ (n = 10; 5 subjects, 2 scans, inter-scan interval < 3
339 weeks). In a leave-one-out analysis by test subject (S_x), group-level SC and FC networks were
340 computed excluding data from both scans, and multi-linear modeling was performed at the
341 pairwise network level. The resultant group-level ß-coefficients were then combined with the
342 unseen subject-level SC data to compute predicted FC, which was correlated with the
343 corresponding empirical FC for both time points using Pearson's correlation ($r_{true} = FC_{predicted}(S_x)$
344 vs $FC_{empirical}(S_x)$). We assessed the significance of r_{true} using a 2-level approach. (1) The ability of
345 the model to produce a general FC pattern was assessed by correlating the predicted FC for S_x

with permuted versions of their empirical FC (n = 1000; $r_{perm} = FC_{predicted}(S_x)$ vs $FC_{empirical\text{-}shuffled}(S_x)$). Shuffling was performed within network pairs to preserve spatial relationships. (2) The ability of the model to produce subject-specific FC patterns was assessed by correlating the predicted FC for S_x with the empirical FC for every other subject y ≠ x ($r_{spec} = FC_{predicted}(S_x)$ vs $FC_{empirical}(S_y)$). For both tests, correlations were performed over all pooled edges (**Figure 6a** and **6b**) and within network pairs (**Figure 6c**). Significance was assessed using one-sided p-values and z-statistics.

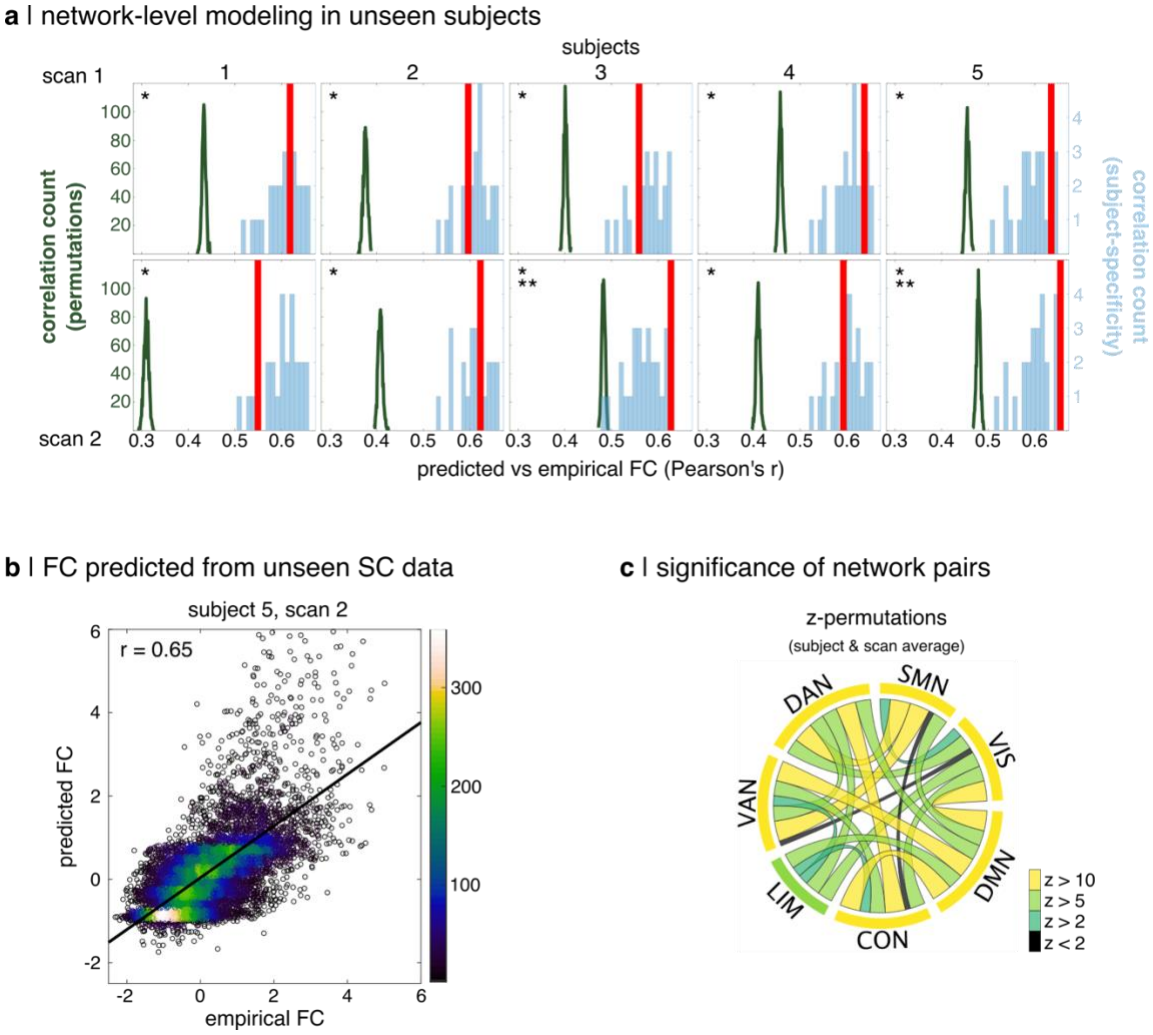

Figure 6. Generalizability and subject-specificity of the full regression model of $BOLD_{in}$ at the network level. ***(a)*** *True correlations of empirical and predicted FC (r_{true}; red bar) are overlaid on the distributions*

of test correlations for generalizability (r_{perm}; forest green) and subject-specificity (r_{spec}; light blue). Single (*) and double asterisks (**) indicate p_{perm} and $p_{spec} < 0.05$, respectively. ***(b)*** *Empirical vs predicted FC for the highest true correlation ($r_{true} = 0.65$).* ***(c)*** *Generalizability significance for each network pair was computed as $z_{perm} = (r_{true} - mean_r_{perm}) / std_r_{perm}$. No network pair showed significant subject-specificity.*

For every subject and scan, r_{true} was significantly higher than r_{perm} ($p_{perm} = 0.001$), indicating that the pattern of predicted FC was more similar to empirical FC than random sequences of FC edges controlling for spatial relationships. In contrast, r_{true} was only significantly higher than r_{spec} for 2 of 10 tests ($p_{spec} = 0.001, 0.041$). When averaging across subjects and scans, r_{true} was significantly higher than r_{perm} ($z > 2$) for nearly every network pair and was an extreme outlier ($z > 10$) for 12 of 29 pairs which included all except the limbic network. No network pairs showed significantly higher r_{true} than r_{spec} (all $z < 1$). Thus, the predicted FC from our multi-linear structural model of function showed strong general patterns of FC but weak subject-specificity.

Sensitivity analyses

Finally, we test the extent to which our results may be sensitive to our specific dataset or processing choices. Our main results showed good consistency when replicated using an independent multi-modal MRI dataset(Royer et al., 2022) to define the structural features and the $BOLD_{in}$ network (**Figure S8**). The edge myelin connectome was quantified using the same method (tractometry) but a different metric in these data ($R_1 = 1/T_1$; longitudinal relaxation rate). We also observed consistency using the lower-resolution Schaefer-200 parcellation (**Figure S6**). All processing steps were identical, except a more conservative threshold was used for consistency-based filtering. In our work, the COMMIT framework was used to derive an estimate of edge caliber, which can be interpreted as quantifying the strength of white matter connectivity. However, the number of streamlines output from streamline tractography is more

often used to quantify SC in structure-function models. To support comparability to previous literature, we additionally show that our results are consistent when using the number of streamlines as an estimate of caliber (**Figure S7)**.

Discussion

The white matter tracts connecting gray matter neuronal populations play a central role in supporting the synchronous neural activity necessary for healthy brain function(Sonya Bells et al., 2017; Filley & Fields, 2016). Yet, we still know very little about the mechanisms mediating this relationship, in part, due to a lack of requisite biological detail in structure-function brain models(Suárez et al., 2020). Here, we provide the most thorough account to date of the relationship between multi-feature white matter structural connectivity and multi-modal functional connectivity. We find that white matter myelin is strongly predictive of FC with coupling patterns that vary regionally and across timescales of neural function.

Mounting evidence supports a role for white matter myelin in mediating macroscale brain function, which complements the established relationship between intracortical myelin and BOLD-FC(Huntenburg et al., 2017). White matter myelin has been used to predict latent components of MEG-FC(Messaritaki et al., 2021). Changes in white matter myelination have been linked causally with disruptions in network connectivity in mouse models(Asleh et al., 2020; Saskia Hübner et al., 2017) and with working memory impairment using computational modeling(Ibañez et al., 2023). Using MRI-based white matter myelin markers, changes in both network myelination(Metzler-Baddeley et al., 2017) and myelin-weighted network topology(Caeyenberghs et al., 2016) have been detected following working memory training. Connectivity networks weighted by white matter myelin have also been shown to differ

405 markedly in topology and correlation with FC from conventional SC networks supporting their
406 complimentary relationships with function(Boshkovski et al., 2021; Nelson et al., 2023). We
407 extend this work by describing in detail how white matter myelin shapes the relationship
408 between structural and functional human brain networks.
409

410 ***White matter myelin as a modulator of structure-function coupling***

411 Structure-function coupling strength was inversely related to the sensory-association axis, in line
412 with previous studies which did not include white matter myelin(Baum et al., 2020; Liu et al.,
413 2023; Osmanlıoğlu et al., 2019; Preti & Van De Ville, 2019; Vázquez-Rodríguez et al., 2019;
414 Wang et al., 2019; Zamani Esfahlani et al., 2022). The oft-observed uncoupling of white matter
415 SC from FC along this gradient is thought to be related to a progressive untethering of the cortex
416 from underlying molecular gradients throughout evolution, which has occurred to the greatest
417 extent in association cortex in humans(Buckner & Krienen, 2013). This — along with a similar
418 pattern in development(Hill et al., 2010) — has been linked to cortical features including
419 myelin(Glasser et al., 2014; Glasser & Van Essen, 2011), cell morphology(Elston, 2003; Glasser
420 & Van Essen, 2011), and transcriptomic alignment(Burt et al., 2018), as well as the genetic
421 heritability of FC(Giles L. Colclough et al., 2017). But what is the role of white matter itself in
422 the uncoupling of SC and FC?

423 Myelin showed the opposite relationship with BOLD and MEG FC across the sensory-
424 association axis relative to caliber and length. We observed consistently strong interactions with
425 white matter myelin for both caliber and length. When stratifying by myelin content, BOLD
426 structure-function coupling was much stronger when myelin was lowest. Both length and caliber
427 uncoupled from BOLD-FC with increasing myelin, while remaining relatively strongly

correlated with each other. These results suggest a role for white matter myelin as a *moderator* of structure-function coupling. When myelin is low, the neural synchrony quantified by FC may be more heavily influenced (i.e., constrained) by other physical properties of white matter connections, such as their length and caliber. Increasing myelination may gradually compensate for variability in these other features, such that a sufficient threshold of myelin has the net effect of equalizing functional synchrony across a diverse range of tract profiles: i.e., a flattening of the structure-function gradient. In other words, white matter myelin may confer functional flexibility or resilience(Noori et al., 2020; Park & Lefebvre, 2020), whether it be to normal or pathological variability in white matter structural properties. Future work may explore this further, e.g., in aging(Slater et al., 2019; Yeatman et al., 2014). Thus, we provide evidence for a modulatory role for white matter myelin in the progressive decoupling of function from its underlying white matter macrostructural constraints, which may contribute to the greater flexibility of brain function characteristic of association networks.

Previous work has established that the fMRI signal is best described by a spatially varying superposition of multiple MEG frequency bands(Shafiei et al., 2022; Tewarie et al., 2016). The modulatory effect of myelin on structure-function coupling was consistent in the out-of-sample BOLD data but was heterogeneous across MEG frequency bands: mostly absent from the gamma bands, and mostly present for low-intermediate frequency bands, although only for edges with the highest myelin content. Taken together, these results suggest that FC for low-to-intermediate frequency MEG may be more strongly constrained by white matter macrostructure, as decoupling is only observed at a higher myelin threshold. Furthermore, FC for high-frequency MEG may be fundamentally decoupled from white matter caliber, which is additionally supported by the relative unimportance of caliber in the prediction of gamma-FC. This is

consistent with a more local and transient nature, which is more strongly dependent on cortical – – as opposed to white matter —structural features(Buzsáki & Wang, 2012). Thus, the stronger modulatory effect observed for BOLD-FC may reflect the filtered integration of heterogeneous modulation of structure-function coupling by white matter myelin across multiple neurophysiological rhythms of brain function.

In sum, we provide robust evidence that white matter myelin has a frequency-dependent modulatory effect on structure-function coupling, which may contribute to the gradual uncoupling of white matter structure and FC along the sensory-association gradient.

Differential roles for white matter myelin in supporting BOLD-FC across the unimodal-transmodal gradient

The FC of a given node pair derived from BOLD-fMRI is an indirect measure of synchronized neural activity, which will intuitively depend on signal transmission speed and distance. Myelin was a stronger predictor of BOLD-FC than length both globally and for most network pairs. On face value, this would suggest that white matter myelin would be a useful proxy for *in vivo* conduction delays; however, previous work has provided evidence to the contrary(Mancini et al., 2021).

Myelin generally showed a balanced relationship with BOLD-FC: mostly negative in unimodal and positive in heteromodal networks. This implies that the strength of neural coupling measured with BOLD-fMRI is associated with lower tract myelination in unimodal and higher myelination in heteromodal networks, which agrees with previous work(Boshkovski et al., 2021; Sydnor et al., 2021). Whereas the hub regions(Martijn P. van den Heuvel & Sporns, 2013) driving the inter-modular integration characteristic of heteromodal networks tend to be

474 connected by long-range white matter tracts, the more segregated processing attributed to
475 unimodal networks tends to be supported by dense local circuits with shorter connections(Betzel
476 & Bassett, 2018; Sepulcre et al., 2010; Sydnor et al., 2021). In this light, our results could
477 indicate that BOLD-FC in heteromodal networks is more reliant on high myelination of white
478 matter connections for temporal coordination between distant brain regions.

479 Alternatively, higher myelination may help reduce the energetic costs of topologically
480 central long-range connections(Bullmore & Sporns, 2012; Harris & Attwell, 2012). A related but
481 separate consideration is adequate trophic support, especially when viewing the insulating effect
482 of myelin from the perspective of metabolic isolation(Nave, 2010). Indeed, mounting evidence
483 suggests that oligodendrocytes directly support axonal energy metabolism independent of their
484 role in modulating conduction velocity(Asadollahi et al., 2024; Fünfschilling et al., 2012; Y. Lee
485 et al., 2012; Narine & Colognato, 2022; Nave et al., 2023; Nave & Werner, 2014; Ramos-Cabrer
486 et al., 2025; Saab et al., 2016). Thus — alongside temporal coordination — both energetics and
487 trophic support may contribute to the observed differential association between myelination and
488 BOLD-FC across the S-A axis.

489

490 ***Connecting white matter and neural synchrony***

491 Our approach provides the unique opportunity to speculate on the interplay between
492 white matter structure and neural synchrony across functional timescales. MEG captures
493 oscillatory neural activity at higher frequencies than BOLD-fMRI and should thus be more
494 sensitive to increasing conduction delays in longer white matter tracts. Indeed, we observed that
495 length increased in importance shifting from BOLD to MEG to become the dominant predictor
496 overall across MEG frequency bands. Myelin also increased in importance and showed

predominantly positive associations in the highest frequency FC. This could be argued to bolster the support of conduction velocity, or perhaps to reflect increasing energy demands at higher frequencies(Lord et al., 2013; Saab et al., 2016; Trevisiol et al., 2017). In line with past work(Hagmann et al., 2008; Koch et al., 2002), caliber dominated the prediction of BOLD-FC showing almost exclusively positive associations. However, as the frequency of brain function increased, caliber decreased in predictive power and shifted to predominantly negative associations with gamma-FC. Taken together, these observations support an intuitive shift in priorities across functional timescales: from higher bandwidth at lower frequencies to greater temporal precision and/or metabolic demands at higher frequencies.

Myelin and length shared dominance in predicting alpha and gamma across network pairs. The association of myelin and FC was inverted between these frequency bands as well: mostly positive in unimodal and negative in heteromodal for $gamma_{hi,}$ and the inverse for alpha. Gamma is associated with local, bottom-up sensory processing and alpha with top-down modulation over longer distances(Baillet, 2017; Fries, 2015; Scheeringa & Fries, 2019). Thus, for intermediate-frequency alpha, the dual-dependence of strong FC on both myelin and length may reflect the role of supporting synchronization over longer distances — as in low-frequency BOLD-FC — alongside a greater reliance on high temporal fidelity. Whereas for high-frequency gamma, the strong dependence of synchrony on physical proximity is evident in the dominance of length, and the significant contribution of myelin reinforces its importance for both timing and metabolic support.

In sum, our results support a frequency-dependent relationship between white matter structure and neural synchrony. In the lowest-frequency BOLD-FC, a global emphasis on bandwidth is suggested by a strong reliance on caliber, and high myelination could be argued to

promote temporal coordination and metabolic support for topologically central long-range connections. As the frequency of FC increases, the global reliance on bandwidth is gradually reduced and eventually overcome by a greater dependence on temporal precision, which is supported by the increasing dominance of length and myelin.

Advantages of a multi-feature, network-level structure-function model

In line with past work(Liu et al., 2023; Zamani Esfahlani et al., 2022), structure-function coupling strength and the correlation of empirical with predicted FC increased when moving from a single global model to smaller regional models. We found the strongest structure-function coupling in limbic network pairs, however the limbic network is typically among the lowest ranked. Previous studies have defined network-level coupling by aggregating over node-level models(Liu et al., 2023; Vázquez-Rodríguez et al., 2019; Zamani Esfahlani et al., 2022), but each node-level model contains edges from multiple network pairs. In contrast, our network-level model focused specifically on edges between pairwise combinations of resting-state networks, which reduced the overall number of models by an order of magnitude and increased the number of data points in each model. Thus, our network-centric approach was more robust, efficient and yielded a more nuanced perspective of structure-function coupling. A complementary but uniquely informative example can be seen in the somatomotor network. Past work has reported strong average structure-function coupling here(Liu et al., 2023; Zamani Esfahlani et al., 2022), and our results generally support this, however with a caveat. The somatomotor network showed no coupling with the limbic and very low coupling strength with control and default mode networks. Therefore, relative to the ventral attention network, which is

typically ranked among the weakest in structure-function coupling, the somatomotor network had lower total coupling strength across all network pairs.

Our analysis also deviated from past work by including multiple white matter structural features and their interactions. Structure-function coupling in BOLD was strongest for network pairs including the visual and dorsal attention networks. The finding in the visual network is corroborated by multiple investigations(Liu et al., 2023; Vázquez-Rodríguez et al., 2019; Zamani Esfahlani et al., 2022), however, the dorsal attention network does not typically rank highly in terms of structure-function coupling strength among resting-state networks(Vázquez-Rodríguez et al., 2019). While most network pairs with the dorsal attention network showed edge caliber as the dominant predictor, large magnitude ß-coefficients were observed for both myelin and length for the network pair with the strongest coupling overall: dorsal attention and limbic. This suggests that the strong structure-function coupling observed with the dorsal attention network in our study may result from our multi-feature approach which included myelin. Another example can be provided using our beta-FC results. While BOLD-FC is best characterized by a mixture of MEG frequency bands, the beta band is thought to be a primary driver of their correspondence(Shafiei et al., 2022). We observed a similar balanced association between myelin and both BOLD and beta FC which showed roughly the same distribution across resting-state networks. In contrast, caliber, length, and both interaction terms showed noticeable differences, suggesting that the strong correspondence between FC in BOLD and beta may be related to overlap in their relationships with white matter myelin. Future work could further explore this possibility using EEG, which is more widely available and also related to SC(Babaeeghazvini et al., 2021).

In sum, the pairwise network-level of analysis yielded a nuanced perspective of regional structure-function coupling while maximizing model robustness and efficiency, and our multi-feature account of white matter structure facilitated deeper interpretation of the relationship between brain structure and function.

Limitations

The principal limitation of this work was the exclusion of some parts of the network from our analysis. (1) Network edges with SC = 0 were excluded, which constitutes more than 80% of the FC network. This is unavoidable when modeling edgewise relationships with structural edge weights directly, as structural brain networks are inherently sparse. This could be addressed in future work using communication modelling(Seguin et al., 2020, 2023). (2) The subcortex and cerebellum were excluded, as these are associated with increased artifact and a lack of standardization for their inclusion in whole brain analyses. (3) Cortical features were excluded in order to focus our analysis on the white matter. Future extensions of this work could integrate these other network components.

A further limitation of the present work is that the MEG FC data were derived from a separate cohort than the structural connectivity used in the modeling. However, all analyses were conducted at the group level, and our interpretations rely on broad population-level trends rather than subject-specific structure–function coupling. We made no inference at the level of individual tracts or anatomical features, and no subject-level predictions were performed using the MEG data. As such, the use of out-of-sample MEG data is unlikely to materially affect the central conclusions. Future work should integrate within-subject multimodal datasets that jointly acquire structural, fMRI, and MEG/EEG measurements. Such data would enable subject-level

analyses of myelin-sensitive communication, allow stronger inferences about individual variability in structure–function coupling, and facilitate testing whether the group-level principles identified here also hold at the level of single participants. In addition, acquiring myelin-sensitive structural measures and electrophysiological activity within the same individuals would enable this framework to be extended to clinical populations with myelin alterations (e.g., demyelinating, neurodevelopmental, or neurodegenerative conditions). Such datasets would make it possible to assess how individual variability in myelin integrity relates to large-scale functional coherence or synchrony, and whether structural disruptions associated with altered myelination are reflected in corresponding changes in electrophysiological coupling.

Another limitation was the use of streamline-tractography and tractometry to compute SC networks. This imparts well known biases(Maier-Hein et al., 2017; Nelson et al., 2023; Schilling et al., 2019). We attempted to mitigate this to the fullest extent possible through careful filtering at both the streamline and connectome levels. We also used a group-consensus approach. This improves the stability of the analysis and focuses on population-level trends at the expense of subject-specificity, e.g., through personalized parcellations(Kong et al., 2021).

Our investigation utilized a single myelin metric derived from MTsat, which provides an estimate of myelin density. Future work could expand on this by measuring myelin with alternate metrics such as the tract g-ratio(Lu et al., 2025; Mancini et al., 2018; Stikov et al., 2015; West et al., 2016). This would provide a complimentary perspective of white matter myelin and further illuminate its coupling with FC. Similarly, future work could expand on the method for estimating caliber e.g., axonal caliber(Barakovic et al., 2021).

Throughout, we have interpreted the sign and magnitude of standardized ß-coefficients in terms of the relationship between predictors (white matter features) and the dependent variable

610 (FC). We recognize that this must be done cautiously, as the ß-coefficients from a given model
611 are sensitive to the predictors included and their collinearity, which is unavoidable in our
612 context. To account for this, all variables were normalized and centered prior to modeling, and
613 dominance analysis was used to quantify relative predictor contributions independent of
614 collinearity.
615

616 ### *Conclusion*

617 This work constitutes the most complete description of the relationship between white matter
618 structural features — including myelin — and functional connectivity across time scales and
619 brain regions. We detail the complex interplay between white matter structure and neural
620 synchrony and describe how it evolves across the neurophysiological rhythms of the brain.
621 Crucially, we provide robust evidence of a frequency-dependent modulatory role for white
622 matter myelin on structure-function coupling along the sensory-association gradient. In all, our
623 contributions highlight the necessity of a multi-feature account of white matter which includes
624 myelin for investigations of the structure-function relationship of the brain.
625

626 ## Materials and Methods

627 ### *Data acquisition*

628 This study was approved by the Research Ethics Board of McGill University, and all participants
629 provided written informed consent. Multi-modal MRI data were collected in a cohort of healthy
630 volunteers (n = 30; 14 men; 29±6 years of age) on a 3 tesla Siemens Magnetom Prisma-Fit
631 scanner equipped with a 64-channel head coil. All sequences used the Siemens *Prescan*

632 *Normalize* option to generate maps with minimal receive B1-field bias. The protocol was as
633 follows:

634 - T_1-weighted (T_1w) anatomical: 3D magnetization-prepared rapid gradient-echo sequence
635 (MP-RAGE; 1.0 mm isotropic; TE/TI/TR = 2.98/900/2300 ms; FA = 9°; iPAT = 2).
636 - T_1 relaxometry: sparse 3D-MP2RAGE(Marques et al., 2010; Mussard et al., 2020)
637 sequence (1.0 mm isotropic; TE/TI_1/TI_2/TR = 2.66/940/2830/5000 ms; FA_1/FA_2 = 4°/5°;
638 TF = 175; undersampling factor = 4.6.
639 - Resting-state fMRI: multiband accelerated 2D-BOLD gradient echo echo-planar
640 sequence (2.6 mm isotropic; TE/TR = 30/746 ms; MB factor = 6; FA = 50°). Two spin-
641 echo images with AP and PA phase encoding were additionally acquired for distortion
642 correction (2.6 mm isotropic; TE/TR = 60.6/6160 ms; FA = 90°).
643 - Magnetization transfer-weighted 3D gradient-echo sequence (1.0 mm isotropic; TE/TR =
644 2.76/27 ms; FA = 6°; iPAT = 2; partial Fourier = 6/8; MT pulse parameters: 12-ms
645 Gaussian pulse, 2kHz off-resonance, $B1_{rms}$ = 3.26μT.
646 - Multi-shell diffusion-weighted imaging (DWI): 2D pulsed gradient spin-echo echo-planar
647 imaging sequence composed of three shells with b-values 300, 1000 and 2000 s/mm^2 and
648 diffusion directions 10, 30, and 64, respectively (2.6 mm isotropic; TE/TR = 57/3000 ms;
649 iPAT = 3; partial Fourier = 6/8). Two b = 0 images with AP and PA phase encoding were
650 additionally acquired to facilitate distortion correction.
651 - A B_1^+ map (2.5 x 2.5 x 3mm^3; TE/TR = 2.22/20k ms; FA = 8°) for ΔB_1^+ correction of
652 MP2RAGE & MTsat maps.

653

654 ***Data processing***

A custom version of the multi-modal processing pipeline *micapipe* (v0.1.5)(Cruces et al., 2022) was used in the processing of all diffusion, anatomical, and functional images. This pipeline makes use of multiple software packages including: *AFNI*(Cox, 1996; Cox & Hyde, 1997), *FSL*(Jenkinson et al., 2012; S. M. Smith et al., 2004; Woolrich et al., 2009), *ANTs*(B. Avants et al., 2009; Brian B. Avants et al., 2014), *FreeSurfer*(Dale et al., 1999; Fischl, 2012; Fischl et al., 2002, 2004; Fischl, Sereno, & Dale, 1999; Fischl, Sereno, Tootell, et al., 1999), and *MRtrix3*(J. D. Tournier et al., 2012, 2019).

T_1w anatomical MRI (MPRAGE). T_1w images were deobliqued, reoriented to standard neuroscience orientation (LPI), N4 bias field corrected(Tustison et al., 2010), intensity normalized, and skull stripped(Hoopes et al., 2022). Model-based segmentation of subcortical structures was performed with FSL FIRST(Patenaude et al., 2011) and tissue types were classified using FSL FAST(Zhang et al., 2001). A five-tissue-type image segmentation was generated for anatomically constrained tractography(R. E. Smith et al., 2012). Cortical surface segmentations were generated with the *FreeSurfer* (v7.2) *recon-all* pipeline with manual edits to remove dura mater.

Resting-state fMRI. After dropping the first 5 TRs from the main scan, all fMRI images (including field maps) were reoriented to standard neuroscience orientation (LPI) and motion corrected within-scan by registering all volumes to their respective temporal mean. Framewise displacement was computed for all main scan volumes, and a threshold (3rd quartile + 1.5 * Interquartile Range) was used to identify volumes with large motion artifacts. The main-phase and reverse-phase field maps were used to correct the main fMRI scan for geometric distortions due to magnetic field inhomogeneity(Andersson et al., 2003; Graham et al., 2017). All subsequent processing involves only the main fMRI scan. Brain extraction(S. M. Smith, 2002)

was performed, followed by registrations to native FreeSurfer space with *bbregister*(Greve & Fischl, 2009) and with the T_1w image using a multi-stage method (rigid, affine, SyN) implemented in ANTs(B. B. Avants et al., 2008).

The fMRI data was denoised by applying a high-pass filter at a cutoff frequency of 0.01 Hz followed by Independent Component Analysis with FSL MELODIC(C.F. Beckmann & Smith, 2004; Christian F. Beckmann et al., 2005). All independent components (n = 3,825) were manually labeled by 2 independent raters, and components labeled as "noise" by both raters were removed (n = 2761). The denoised data was then used to calculate tissue-specific signals for gray matter, white matter, and cerebrospinal fluid tissue classes, before being mapped to native surface space and smoothed (Gaussian, FWHM = 6 mm). Linear regression was applied to the surface-based time series to remove nuisance signal resulting from motion, cerebrospinal fluid or white matter tissue.

Multi-shell DWI. The DWI data including field maps (b = 0 s/mm^2 volumes with reverse phase encoding) were denoised(Cordero-Grande et al., 2019; Veraart, Fieremans, et al., 2016; Veraart, Novikov, et al., 2016), then corrected for Gibbs ringing(H. Lee et al., 2021). The field maps were then used to correct for susceptibility distortion, head motion, and eddy currents via FSL's TOPUP(Andersson et al., 2003) and eddy(Andersson & Sotiropoulos, 2016). This was followed by B1$^+$ bias-field correction(Tustison et al., 2010). The corrected DWI image was upsampled to match the T1w resolution (1 mm isotropic), and brain extraction was performed(S. M. Smith, 2002). These preprocessed data were used to estimate multi-shell and multi-tissue response functions(Christiaens et al., 2015; Dhollander et al., 2016, 2019), which informed the estimation of fiber orientation distributions (FOD) via spherical deconvolution(Jeurissen et al., 2014). All FODs were intensity normalized(Dhollander et al., 2021). A multi-stage (rigid, affine,

SyN) registration(B. B. Avants et al., 2008) was computed with the T_1w image to allow co-registration of anatomical images to DWI space.

T_1 relaxometry and magnetization transfer saturation (MTsat) maps. A dictionary matching approach incorporating the B_1^+ map was applied to generate S_0 and T_1 maps from the MP2RAGE inversion 1, inversion 2 and UNI images. This produced ΔB_1^+ corrected S_0 & T_1 maps. An affine transformation (ANTs) was used to register the MP2RAGE denoised UNI image, the S_0 and T_1 maps, and the MT-weighted image to the T_1w image. MTsat maps were computed using(Helms et al., 2008):

$$MTsat = \left(\frac{S0 \cdot \alpha \cdot \Delta B_1^+}{S_{MT_w}} - 1\right) \cdot \frac{TR}{T1} - \frac{(\alpha \cdot \Delta B_1^+)^2}{2} \quad (1)$$

where α is the excitation flip angle in the MT-weighted sequence, S_{MTw} is the MT-weighted signal, and TR is the repetition time of the MT-weighted sequence. A gain factor of 2.5 was applied to the S_0 maps to match the receiver gain of the MT-weighted gradient echo sequence for computing MTsat. ΔB_1^+ was corrected using a model-based approach(Rowley et al., 2021).

Structural connectivity network reconstruction

Tractography and filtering. Anatomically constrained(R. E. Smith et al., 2012) tractography was run on the normalized white matter FOD with the probabilistic algorithm iFOD2(J.-D. Tournier et al., 2010) and a dynamic seeding strategy(R. E. Smith et al., 2015) to generate tractograms of 3 million streamlines. All tractograms were filtered in a multi-stage process (see(Lu et al., 2025) for more detail):

1. Any erroneous streamlines that failed to connect two gray matter ROIs were manually removed to ensure they did not bias the model in step 2.

2. COMMIT v2.1(Daducci et al., 2013, 2015) (convex optimization modeling for microstructure informed tractography) was run on the stage-1 filtered tractograms. COMMIT evaluates the contribution of each streamline to the measured diffusion signal and assigns weights that best reconstruct the voxel-wise diffusion profile. Streamlines which are not supported by the underlying microstructure are down-weighted or eliminated. COMMIT was optimized to the DWI image using a Stick-Zeppelin-Ball forward model with diffusivities $Đ_{\parallel} = 1.7e^{-3}$, $Đ_{\perp} = 0.51e^{-3}$ and $Đ_{iso} = 1.7e^{-3}, 3.0e^{-3}$ mm^2/s (gray matter and CSF). Estimates of the signal fraction or intra-cellular volume fraction (ICVF) of each streamline were extracted from the COMMIT model. Streamlines < $1e^{-12}$ were filtered as they did not contribute to the global DWI signal. A volumetric ICVF map was also obtained from COMMIT. This was used to calibrate the MT_{sat} map yielding a myelin volume fraction (MVF) map as:

$$MVF = \alpha_{calib} \times MT_{sat} \tag{2}$$

where α_{calib} is the global calibration factor as described in(Lu et al., 2025).

3. The stage-2 filtered tractograms were optimized to the MVF map with a myelin-based COMMIT extension(Schiavi et al., 2022) yielding a signal fraction for each streamline which corresponded to a myelin cross-sectional area. Streamlines < $1e^{-12}$ were filtered as they did not contribute to the global MVF signal.
4. To get the final signal fraction (ICVF) for the surviving streamlines, a modified version of step 2 was repeated on the stage-3 filtered tractograms. Instead of optimizing COMMIT to the DWI signal itself, a scaled version was computed (1-MVF), which was then normalized by the b = 0 images. This was done to account for the potential bias of

myelination to the ICVF estimates from COMMIT. A very small number of streamlines $< 1e^{-12}$ were filtered in this stage as well.

These filtered tractograms were used for all structural connectomes i.e., both the underlying streamlines and edge connection density were uniform across all variants of weighted structural connectomes. Although our filtering pipeline made it possible to estimate a connectome weighted by tract-specific MVF, such a myelin metric is highly collinear with edge caliber (derived from COMMIT in our analysis), which would represent a significant confound in our multiple regression framework. Thus, these were not used in this study. Instead, we are estimating edge myelin density using MTsat tractometry, which is more complementary to edge caliber (Figure S10).

Weighted structural connectomes. The edge *caliber* connectome was computed by summing the final COMMIT weights (signal fractions) of all remaining streamlines connecting each node pair normalized by total node volume for each pair. The edge *myelin* connectome was computed by applying tractometry(S Bells et al., 2011) to the MTsat image: the median MTsat value was computed along each streamline, followed by the average across streamlines for each node pair. The edge *length* connectome was computed as the mean length of streamlines for each node pair. The Schaefer-400(Schaefer et al., 2018) cortical atlas was used to define network nodes in all primary analyses.

Group-consensus structural connectomes. We developed a group averaging method through rigorous testing to maximally preserve subject-level features. This was carried out in a two-stage process. (1) Consistency-based filtering(Roberts et al., 2017) targeted to cross-subject variance in number of streamlines edge weights was used to filter all subject-level structural connectomes to a threshold of 30% (the final density if averaging was performed at this stage).

768 (2) Distance-dependent thresholding(Betzel et al., 2019) was then applied to generate group-
769 representative structural connectomes which preserved subject-level within- and between-
770 hemisphere edge length distributions. Final group-level connection density was 23%, which was
771 approximately the median subject-level density.
772

773 ***Functional connectivity network reconstruction***

774 Functional connectivity was computed as the zero-lag Pearson cross-correlation of fMRI time
775 series. These values were Fisher z-transformed and averaged across subjects yielding a single in-
776 sample-fMRI functional connectome in the Schaefer-400 parcellation.

777 **HCP data.** Fully-processed fMRI and MEG functional connectivity matrices were
778 obtained at the group-level in the Schaefer-400 parcellation. These connectomes were derived
779 from resting-state data acquired in healthy young adults (n = 33; age range 22 to 35 years) as part
780 of the Human Connectome Project (HCP; S900 release(Van Essen et al., 2013)). In a previous
781 study(Shafiei et al., 2022), these specific datasets were selected from the small proportion of the
782 full cohort which contained MEG data for unrelated subjects, and we elected to reuse these same
783 data as the number of participants and their age range matched closely to our in-house data
784 sample. The MEG data corresponded to 6 minutes of scanning (sampling rate = 2,034.5 Hz; anti-
785 aliasing low-pass filter = 400 Hz), and the fMRI data were comprised of 4 scans of 15 minutes
786 across 2 sessions (TR = 720 ms; 3 Tesla; 2 mm isotropic). Static functional connectivity was
787 computed as (1) the Pearson cross-correlation of fMRI time series and (2) the amplitude
788 envelope correlation(Bruns et al., 2000) of MEG time series data. An orthogonalization process
789 was then applied to correct for spatial leakage in the MEG functional connectomes(G. L.
790 Colclough et al., 2015). Group-averaging yielded one fMRI and six MEG functional

connectomes corresponding to the canonical electrophysiological frequency bands: delta (δ: 2-4 Hz), theta (θ: 5-7 Hz), alpha (α: 8-12 Hz), beta (β: 15-29 Hz), low gamma (γ_{lo}: 30-59 Hz), and high gamma (γ_{hi}: 60-90Hz). See(Shafiei et al., 2022) for full processing details.

Multi-linear modeling

We quantified the role of white matter features in predicting synchronized brain function using multiple linear regression. The dependent variable (response variable) was functional connectivity (FC) from one of the following modalities: in-sample-fMRI ($BOLD_{in}$), HCP-fMRI ($BOLD_{out}$) or HCP-MEG in the 6 canonical frequency bands (n = 8 unique dependent variables). The predictors were structural connectivity (SC) weights quantifying the *caliber*, *myelin* and *length* of each edge. Interaction terms were included for both caliber and length with myelin. Only edges with SC ≠ 0 were included. The *adjusted* R^2 (coefficient of determination) was interpreted as the magnitude of structure-function coupling. The contribution of each predictor was quantified with dominance analysis(Azen & Budescu, 2003; Budescu, 1993), which measures relative predictor importance as the incremental change in R^2 from the addition (or absence) of a given predictor to all possible subset models. Dominance analysis was adapted to handle interaction terms for this work. Variables with an absolute skewness > 1.5 were log-transformed, and all variables were z-scored. Modeling was restricted to group-level data. Parametric t-tests were used to exclude any ß-coefficients with $p > 0.05$.

Global model. The whole-brain linear regression model was computed as:

$$FC_k = 1 \quad + \quad caliber * myelin \quad + \quad length * myelin \tag{3}$$

where the predictors *caliber*, *myelin* and *length* are the vectorized lower triangle elements of the corresponding weighted structural connectome, and the dependent variable FC_k is the corresponding vectorized lower triangle elements of the kth FC dataset.

Network model. Nodes (cortical parcels) were grouped by affiliation to the 7-canonical resting state sub-networks(Thomas Yeo et al., 2011), and linear regression was performed within pairwise combinations of sub-networks as:

$$FC_k^{ij} = 1 + caliber^{ij} * myelin^{ij} + length^{ij} * myelin^{ij} \quad (4)$$

where the FC and SC data corresponded to the weights of network edges linking the nodes of subnetworks i and j. Within-subnetwork modeling is quantified by the case where $i = j$.

Node model. Linear regression was performed separately for each node as:

$$FC_k^{i} = 1 + caliber^{i} * myelin^{i} + length^{i} * myelin^{i} \quad (5)$$

where the FC and SC data corresponded to the weights of network edges linking node i to all other $j \neq i$ nodes.

Null models

To account for the lack of strictness of parametric t-tests applied to our data, we additionally assessed the significance of our results using edgewise permutation testing with 1000 repetitions. When testing the model outputs, the FC edge weights were shuffled to ensure the relationships between the structural predictors were preserved. For the global model, a spatial constraint was added to the permutation test by shuffling FC edge weights within 10 equally sized bins defined by Euclidean distance. One-sided p-values were computed in which the empirical value was included in the null distribution to avoid $p_{perm} = 0$.

Data availability

All data necessary to replicate this work are freely available at https://github.com/TardifLab/Modeling-Myelin-FC.

Code availability

All code necessary to replicate this work are freely available at https://github.com/TardifLab/Modeling-Myelin-FC.

References

Andersson, J. L. R., Skare, S., & Ashburner, J. (2003). How to correct susceptibility distortions in spin-echo echo-planar images: Application to diffusion tensor imaging. *NeuroImage*, *20*(2), 870–888. https://doi.org/10.1016/S1053-8119(03)00336-7

Andersson, J. L. R., & Sotiropoulos, S. N. (2016). An integrated approach to correction for off-resonance effects and subject movement in diffusion MR imaging. *NeuroImage*, *125*, 1063–1078. https://doi.org/10.1016/j.neuroimage.2015.10.019

Asadollahi, E., Trevisiol, A., Saab, A. S., Looser, Z. J., Dibaj, P., Ebrahimi, R., Kusch, K., Ruhwedel, T., Möbius, W., Jahn, O., Lee, J. Y., Don, A. S., Khalil, M. A., Hiller, K., Baes, M., Weber, B., Abel, E. D., Balabio, A., Popko, B., … Nave, K. A. (2024). Oligodendroglial fatty acid metabolism as a central nervous system energy reserve. *Nature Neuroscience*, *27*(October). https://doi.org/10.1038/s41593-024-01749-6

Asleh, J., Shofty, B., Cohen, N., Kavushansky, A., López-Juárez, A., Constantini, S., Ratner, N., & Kahn, I. (2020). Brain-wide structural and functional disruption in mice with oligodendrocyte-specific Nf1 deletion is rescued by inhibition of nitric oxide synthase. *Proceedings of the National Academy of Sciences of the United States of America*, *117*(36), 22506–22513. https://doi.org/10.1073/pnas.2008391117

Assaf, Y., Blumenfeld-Katzir, T., Yovel, Y., & Basser, P. J. (2008). AxCaliber: A method for measuring axon diameter distribution from diffusion MRI. *Magnetic Resonance in Medicine*, *59*(6), 1347–1354. https://doi.org/10.1002/mrm.21577

Avants, B. B., Epstein, C. L., Grossman, M., & Gee, J. C. (2008). Symmetric diffeomorphic image registration with cross-correlation: Evaluating automated labeling of elderly and neurodegenerative brain. *Medical Image Analysis*, *12*(1), 26–41. https://doi.org/10.1016/j.media.2007.06.004

Avants, B., Tustison, N., & Johnson, H. (2009). Advanced Normalization Tools (ANTS). *Insight Journal*, 1–35.

Avants, Brian B., Tustison, N. J., Stauffer, M., Song, G., Wu, B., & Gee, J. C. (2014). The Insight ToolKit image registration framework. *Frontiers in Neuroinformatics*, *8*(APR), 1–13. https://doi.org/10.3389/fninf.2014.00044

Azen, R., & Budescu, D. V. (2003). The Dominance Analysis Approach for Comparing Predictors in Multiple Regression. *Psychological*

Methods, *8*(2), 129–148. https://doi.org/10.1037/1082-989X.8.2.129

Azevedo, F. A. C., Carvalho, L. R. B., Grinberg, L. T., Farfel, J. M., Ferretti, R. E. L., Leite, R. E. P., Filho, W. J., Lent, R., & Herculano-Houzel, S. (2009). Equal numbers of neuronal and nonneuronal cells make the human brain an isometrically scaled-up primate brain. *Journal of Comparative Neurology*, *513*(5), 532–541. https://doi.org/10.1002/cne.21974

Babaeeghazvini, P., Rueda-Delgado, L. M., Gooijers, J., Swinnen, S. P., & Daffertshofer, A. (2021). Brain Structural and Functional Connectivity: A Review of Combined Works of Diffusion Magnetic Resonance Imaging and Electro-Encephalography. *Frontiers in Human Neuroscience*, *15*(October). https://doi.org/10.3389/fnhum.2021.721206

Bacmeister, C. M., Huang, R., Osso, L. A., Thornton, M. A., Conant, L., Chavez, A. R., Poleg-Polsky, A., & Hughes, E. G. (2022). Motor learning drives dynamic patterns of intermittent myelination on learning-activated axons. *Nature Neuroscience*, *25*(10), 1300–1313. https://doi.org/10.1038/s41593-022-01169-4

Baillet, S. (2017). Magnetoencephalography for brain electrophysiology and imaging. *Nature Neuroscience*, *20*(3), 327–339. https://doi.org/10.1038/nn.4504

Barakovic, M., Tax, C. M. W., Rudrapatna, U., Chamberland, M., Rafael-Patino, J., Granziera, C., Thiran, J. P., Daducci, A., Canales-Rodríguez, E. J., & Jones, D. K. (2021). Resolving bundle-specific intra-axonal T2 values within a voxel using diffusion-relaxation tract-based estimation. *NeuroImage*, *227*(September 2020), 117617. https://doi.org/10.1016/j.neuroimage.2020.117617

Basser, P. J., Mattiello, J., & LeBihan, D. (1994). MR diffusion tensor spectroscopy and imaging. *Biophysical Journal*, *66*(1), 259–267. https://doi.org/10.1016/S0006-3495(94)80775-1

Bassett, D. S., & Sporns, O. (2017). Network neuroscience. In *Nature Neuroscience* (Vol. 20, Issue 3, pp. 353–364). Nature Publishing Group. https://doi.org/10.1038/nn.4502

Baum, G. L., Cui, Z., Roalf, D. R., Ciric, R., Betzel, R. F., Larsen, B., Cieslak, M., Cook, P. A., Xia, C. H., Moore, T. M., Ruparel, K., Oathes, D. J., Alexander-Bloch, A. F., Shinohara, R. T., Raznahan, A., Gur, R. E., Gur, R. C., Bassett, D. S., & Satterthwaite, T. D. (2020). Development of structure–function coupling in human brain networks during youth. *Proceedings of the National Academy of Sciences of the United States of America*, *117*(1), 771–778. https://doi.org/10.1073/pnas.1912034117

Beckmann, C.F., & Smith, S. M. (2004). Probabilistic Independent Component Analysis for Functional Magnetic Resonance Imaging. *IEEE Transactions on Medical Imaging*, *23*(2), 137–152. https://doi.org/10.1109/TMI.2003.822821

Beckmann, Christian F., DeLuca, M., Devlin, J. T., & Smith, S. M. (2005). Investigations into resting-state connectivity using independent component analysis. *Philosophical Transactions of the Royal Society B: Biological Sciences*, *360*(1457), 1001–1013. https://doi.org/10.1098/rstb.2005.1634

Bells, S, Cercignani, M., Deoni, S., & Assaf, Y. (2011). "Tractometry" – comprehensive multi-modal quantitative assessment of white matter along specific tracts. *Proceedings of the International Society for Magnetic Resonance in Medicine*, *19*(2009), 678. http://cds.ismrm.org/protected/11MProceedings/files/678.pdf

Bells, Sonya, Lefebvre, J., Prescott, S. A., Dockstader, C., Bouffet, E., Skocic, J., Laughlin, S., & Mabbott, D. J. (2017). Changes in white matter microstructure impact cognition by disrupting the ability of neural assemblies to synchronize. *Journal of Neuroscience*, *37*(34), 8227–8238. https://doi.org/10.1523/jneurosci.0560-17.2017

Berman, S., Filo, S., & Mezer, A. A. (2019). Modeling conduction delays in the corpus callosum using MRI-measured g-ratio. *NeuroImage*, *195*,

128–139. https://doi.org/10.1016/j.neuroimage.2019.03.025

Betzel, R. F., & Bassett, D. S. (2018). Specificity and robustness of long-distance connections in weighted, interareal connectomes. *Proceedings of the National Academy of Sciences of the United States of America*, *115*(21), E4880–E4889. https://doi.org/10.1073/pnas.1720186115

Betzel, R. F., Griffa, A., Hagmann, P., & Misic, B. (2019). Distance-dependent consensus thresholds for generating group-representative structural brain networks. *Network Neuroscience*, *3*(2), 475–496. https://doi.org/https://doi.org/10.1162/ netn_a_00075

Biswal, B., Zerrin Yetkin, F., Haughton, V. M., & Hyde, J. S. (1995). Functional connectivity in the motor cortex of resting human brain using echo-planar mri. *Magnetic Resonance in Medicine*, *34*(4), 537–541. https://doi.org/10.1002/mrm.1910340409

Boshkovski, T., Kocarev, L., Cohen-Adad, J., Mišić, B., Lehéricy, S., Stikov, N., & Mancini, M. (2021). The R1-weighted connectome: complementing brain networks with a myelin-sensitive measure. *Network Neuroscience*, *5*(2), 358–372. https://doi.org/10.1162/netn_a_00179

Brookes, M. J., Tewarie, P. K., Hunt, B. A. E., Robson, S. E., Gascoyne, L. E., Liddle, E. B., Liddle, P. F., & Morris, P. G. (2016). A multi-layer network approach to MEG connectivity analysis. *NeuroImage*, *132*, 425–438. https://doi.org/10.1016/j.neuroimage.2016.02.045

Bruns, A., Eckhorn, R., Jokeit, H., & Ebner, A. (2000). Amplitude envelope correlation detects coupling among incoherent brain signals. *NeuroReport*, *11*(7), 1509–1514. https://doi.org/10.1097/00001756-200005150-00029

Buckner, R. L., & Krienen, F. M. (2013). The evolution of distributed association networks in the human brain. *Trends in Cognitive Sciences*, *17*(12), 648–665. https://doi.org/10.1016/j.tics.2013.09.017

Budescu, D. V. (1993). Dominance analysis: A new approach to the problem of relative importance of predictors in multiple regression. *Psychological Bulletin*, *114*(3), 542–551. https://doi.org/10.1037/0033-2909.114.3.542

Bullmore, E., & Sporns, O. (2012). The economy of brain network organization. *Nature Reviews Neuroscience*, *13*(5), 336–349. https://doi.org/10.1038/nrn3214

Burt, J. B., Demirtaş, M., Eckner, W. J., Navejar, N. M., Ji, J. L., Martin, W. J., Bernacchia, A., Anticevic, A., & Murray, J. D. (2018). Hierarchy of transcriptomic specialization across human cortex captured by structural neuroimaging topography. *Nature Neuroscience*, *21*(9), 1251–1259. https://doi.org/0.1038/s41593-018-0195-0.

Buzsáki, G., & Wang, X. J. (2012). Mechanisms of gamma oscillations. *Annual Review of Neuroscience*, *35*, 203–225. https://doi.org/10.1146/annurev-neuro-062111-150444

Caeyenberghs, K., Metzler-Baddeley, C., Foley, S., & Jones, D. K. (2016). Dynamics of the human structural connectome underlying working memory training. *Journal of Neuroscience*, *36*(14), 4056–4066. https://doi.org/10.1523/JNEUROSCI.1973-15.2016

Chaudhuri, R., Knoblauch, K., Gariel, M. A., Kennedy, H., & Wang, X. J. (2015). A Large-Scale Circuit Mechanism for Hierarchical Dynamical Processing in the Primate Cortex. *Neuron*, *88*(2), 419–431. https://doi.org/10.1016/j.neuron.2015.09.008

Chorghay, Z., Káradóttir, R. T., & Ruthazer, E. S. (2018). White matter plasticity keeps the brain in tune: Axons conduct while glia wrap. *Frontiers in Cellular Neuroscience*, *12*(November), 1–15. https://doi.org/10.3389/fncel.2018.00428

Christiaens, D., Reisert, M., Dhollander, T., Sunaert, S., Suetens, P., & Maes, F. (2015). Global tractography of multi-shell diffusion-weighted imaging data using a multi-tissue model. *NeuroImage*, *123*, 89–101. https://doi.org/10.1016/j.neuroimage.2015.08.008

Colclough, G. L., Brookes, M. J., Smith, S. M., & Woolrich, M. W. (2015). A symmetric multivariate leakage correction for MEG connectomes. *NeuroImage*, *117*, 439–448. https://doi.org/10.1016/j.neuroimage.2015.03.071

Colclough, Giles L., Smith, S. M., Nichols, T. E., Winkler, A. M., Sotiropoulos, S. N., Glasser, M. F., Van Essen, D. C., & Woolrich, M. W. (2017). The heritability of multi-modal connectivity in human brain activity. *ELife*, *6*, 1–19. https://doi.org/10.7554/eLife.20178

Cordero-Grande, L., Christiaens, D., Hutter, J., Price, A. N., & Hajnal, J. V. (2019). Complex diffusion-weighted image estimation via matrix recovery under general noise models. *NeuroImage*, *200*(March), 391–404. https://doi.org/10.1016/j.neuroimage.2019.06.039

Cox, R. W. (1996). AFNI: Software for analysis and visualization of functional magnetic resonance neuroimages. *Computers and Biomedical Research*, *29*(3), 162–173. https://doi.org/10.1006/cbmr.1996.0014

Cox, R. W., & Hyde, J. S. (1997). Software tools for analysis and visualization of fMRI data. *NMR in Biomedicine*, *10*(4–5), 171–178. https://doi.org/10.1002/(SICI)1099-1492(199706/08)10:4/5<171::AID-NBM453>3.0.CO;2-L

Cruces, R. R., Royer, J., Herholz, P., Larivière, S., Vos de Wael, R., Paquola, C., Benkarim, O., Park, B., Degré-Pelletier, J., Nelson, M. C., DeKraker, J., Leppert, I. R., Tardif, C., Poline, J.-B., Concha, L., & Bernhardt, B. C. (2022). Micapipe: A pipeline for multimodal neuroimaging and connectome analysis. *NeuroImage*, *263*(August), 119612. https://doi.org/10.1016/j.neuroimage.2022.119612

Daducci, A., Dal Palu, A., Lemkaddem, A., & Thiran, J. P. (2013). A convex optimization framework for global tractography. *Proceedings - International Symposium on Biomedical Imaging*, 524–527. https://doi.org/10.1109/ISBI.2013.6556527

Daducci, A., Dal Palù, A., Lemkaddem, A., & Thiran, J. P. (2015). COMMIT: Convex optimization modeling for microstructure informed tractography. *IEEE Transactions on Medical Imaging*, *34*(1), 246–257. https://doi.org/10.1109/TMI.2014.2352414

Dale, A. M., Fischl, B., & Sereno, M. I. (1999). Cortical Surface-Based Analysis. *NeuroImage*, *9*(2), 179–194. https://doi.org/10.1006/nimg.1998.0395

Deligianni, F., Carmichael, D. W., Zhang, G. H., Clark, C. A., & Clayden, J. D. (2016). NODDI and tensor-based microstructural indices as predictors of functional connectivity. *PLoS ONE*, *11*(4), 1–17. https://doi.org/10.1371/journal.pone.0153404

Dhollander, T., Mito, R., Raffelt, D., & Connelly, A. (2019). Improved white matter response function estimation for 3-tissue constrained spherical deconvolution. *Proc. Intl. Soc. Mag. Reson. Med*, *May 11-16*, 555. https://www.researchgate.net/publication/331165168_Improved_white_matter_response_function_estimation_for_3-tissue_constrained_spherical_deconvolution

Dhollander, T., Raffelt, D., & Connelly, A. (2016). Unsupervised 3-tissue response function estimation from single-shell or multi-shell diffusion MR data without a co-registered T1 image Predicting stroke impairment using machine learning techniques View project A novel sparse partial correlation method fo. *ISMRM Workshop on Breaking the Barriers of Diffusion MRI*, *35*(September), 1–2. https://www.researchgate.net/publication/307863133

Dhollander, T., Tabbara, R., Rosnarho-Tornstrand, J., Tournier, J.-D., Raaelt, D., & Connelly, A. (2021). Multi-tissue log-domain intensity and inhomogeneity normalisation for quantitative apparent density. *ISMRM 29*, 2472. https://doi.org/10.31219/osf.io/zu8fv

Douglas Fields, R. (2015). A new mechanism of nervous system plasticity: activity-dependent myelination. *Nature Reviews Neuroscience*, *16*(12), 756–767. https://doi.org/10.1007/s11065-015-9294-9.Functional

Elston, G. N. (2003). Cortex, Cognition and the Cell: New Insights into the Pyramidal Neuron and Prefrontal Function. *Cerebral Cortex*, *13*(11), 1124–1138. https://doi.org/10.1093/cercor/bhg093

Fields, R. D., Woo, D. H., & Basser, P. J. (2015). Glial regulation of the neuronal connectome through local and long-distant communication. *Neuron*, *86*(2), 374–386. https://doi.org/10.1016/j.neuron.2015.01.014

Filley, C. M., & Fields, R. D. (2016). White matter and cognition: Making the connection. *Journal of Neurophysiology*, *116*(5), 2093–2104. https://doi.org/10.1152/jn.00221.2016

Fischl, B. (2012). FreeSurfer. *NeuroImage*, *62*(2), 774–781. https://doi.org/10.1016/j.neuroimage.2012.01.021

Fischl, B., Salat, D. H., Busa, E., Albert, M., Dieterich, M., Haselgrove, C., Van Der Kouwe, A., Killiany, R., Kennedy, D., Klaveness, S., Montillo, A., Makris, N., Rosen, B., & Dale, A. M. (2002). Whole brain segmentation: Automated labeling of neuroanatomical structures in the human brain. *Neuron*, *33*(3), 341–355. https://doi.org/10.1016/S0896-6273(02)00569-X

Fischl, B., Sereno, M. I., & Dale, A. M. (1999). Cortical surface-based analysis: II. Inflation, flattening, and a surface-based coordinate system. *NeuroImage*, *9*(2), 195–207. https://doi.org/10.1006/nimg.1998.0396

Fischl, B., Sereno, M. I., Tootell, R. B. H., & Dale, A. M. (1999). High-resolution intersubject averaging and a coordinate system for the cortical surface. *Human Brain Mapping*, *8*(4), 272–284. https://doi.org/10.1002/(SICI)1097-0193(1999)8:4<272::AID-HBM10>3.0.CO;2-4

Fischl, B., Van Der Kouwe, A., Destrieux, C., Halgren, E., Ségonne, F., Salat, D. H., Busa, E., Seidman, L. J., Goldstein, J., Kennedy, D., Caviness, V., Makris, N., Rosen, B., & Dale, A. M. (2004). Automatically Parcellating the Human Cerebral Cortex. *Cerebral Cortex*, *14*(1), 11–22. https://doi.org/10.1093/cercor/bhg087

Florin, E., & Baillet, S. (2015). The brain's resting-state activity is shaped by synchronized cross-frequency coupling of neural oscillations. *NeuroImage*, *111*, 26–35. https://doi.org/10.1016/j.neuroimage.2015.01.054

Fornito, A., Zalesky, A., & Bullmore, E. T. (2016). Fundamentals of Brain Network Analysis. In *Fundamentals of Brain Network Analysis*. Elsevier. https://doi.org/10.1016/C2012-0-06036-X

Fries, P. (2015). Rhythms for Cognition: Communication through Coherence. *Neuron*, *88*(1), 220–235. https://doi.org/10.1016/j.neuron.2015.09.034

Fünfschilling, U., Supplie, L. M., Mahad, D., Boretius, S., Saab, A. S., Edgar, J., Brinkmann, B. G., Kassmann, C. M., Tzvetanova, I. D., Möbius, W., Diaz, F., Meijer, D., Suter, U., Hamprecht, B., Sereda, M. W., Moraes, C. T., Frahm, J., Goebbels, S., & Nave, K. A. (2012). Glycolytic oligodendrocytes maintain myelin and long-term axonal integrity. *Nature*, *485*(7399), 517–521. https://doi.org/10.1038/nature11007

Fuster, J. M. (1995). Gradients of Cortical Plasticity. In *Brain and Memory: Modulation and Mediation of Neuroplasticity*. Oxford University Press. https://doi.org/10.1093/acprof:oso/9780195082944.003.0015

Fuster, J. M. (2008). *The prefrontal cortex* (4th ed., Vol. 4). Elsevier.

Garcés, P., Pereda, E., Hernández-Tamames, J. A., Del-Pozo, F., Maestú, F., & Ángel Pineda-Pardo, J. (2016). Multimodal description of whole brain connectivity: A comparison of resting state MEG, fMRI, and DWI. *Human Brain Mapping*, *37*(1), 20–34. https://doi.org/10.1002/hbm.22995

Gast, H., & Assaf, Y. (2024). Weighting the structural connectome: Exploring its impact on network properties and predicting cognitive performance in the human brain. *Network Neuroscience*, *8*(1), 119–137. https://doi.org/10.1162/netn_a_00342

Glasser, M. F., Goyal, M. S., Preuss, T. M., Raichle, M. E., & Van Essen, D. C. (2014). Trends and properties of human cerebral cortex: Correlations with cortical myelin content. *NeuroImage*, *93*, 165–175. https://doi.org/10.1016/j.neuroimage.2013.03.060

Glasser, M. F., & Van Essen, D. C. (2011). Mapping Human Cortical Areas In Vivo Based on Myelin Content as Revealed by T1- and T2-Weighted MRI. *Journal of Neuroscience*, *31*(32), 11597–11616. https://doi.org/10.1523/JNEUROSCI.2180-11.2011

Gong, Z., Bilgel, M., An, Y., Bergeron, C. M., Bergeron, J., Zukley, L., Ferrucci, L., Resnick, S. M., & Bouhrara, M. (2024). Cerebral white matter myelination is associated with longitudinal changes in processing speed across the adult lifespan. *Brain Communications*, *6*(6), 1–15. https://doi.org/10.1093/braincomms/fcae412

Goriely, A. (2025). Eighty-six billion and counting: do we know the number of neurons in the human brain? *Brain : A Journal of Neurology*, *148*(3), 689–691. https://doi.org/10.1093/brain/awae390

Graham, M. S., Drobnjak, I., Jenkinson, M., & Zhang, H. (2017). Quantitative assessment of the susceptibility artefact and its interaction with motion in diffusion MRI. *PLoS ONE*, *12*(10), 1–25. https://doi.org/10.1371/journal.pone.0185647

Greve, D. N., & Fischl, B. (2009). Accurate and robust brain image alignment using boundary-based registration. *NeuroImage*, *48*(1), 63–72. https://doi.org/10.1016/j.neuroimage.2009.06.060

Hagmann, P., Cammoun, L., Gigandet, X., Meuli, R., Honey, C. J., Van Wedeen, J., & Sporns, O. (2008). Mapping the structural core of human cerebral cortex. *PLoS Biology*, *6*(7), 1479–1493. https://doi.org/https://doi.org/10.1371/journal.pbio.0060159

Hansen, J. Y., Shafiei, G., Markello, R. D., Smart, K., Cox, S. M. L., Nørgaard, M., Beliveau, V., Wu, Y., Gallezot, J., Aumont, É., Servaes, S., Scala, S. G., DuBois, J. M., Wainstein, G., Bezgin, G., Funck, T., Schmitz, T. W., Spreng, R. N., Galovic, M., … Misic, B. (2022). Mapping neurotransmitter systems to the structural and functional organization of the human neocortex. *Nature Neuroscience*, *25*(11), 1569–1581. https://doi.org/10.1038/s41593-022-01186-3

Harris, J. J., & Attwell, D. (2012). The energetics of CNS white matter. *Journal of Neuroscience*, *32*(1), 356–371. https://doi.org/10.1523/JNEUROSCI.3430-11.2012

Helbling, S., Teki, S., Callaghan, M. F., Sedley, W., Mohammadi, S., Griffiths, T. D., Weiskopf, N., & Barnes, G. R. (2015). Structure predicts function: Combining non-invasive electrophysiology with in-vivo histology. *NeuroImage*, *108*, 377–385. https://doi.org/10.1016/j.neuroimage.2014.12.030

Helms, G., Dathe, H., Kallenberg, K., & Dechent, P. (2008). High-resolution maps of magnetization transfer with inherent correction for RF inhomogeneity and T1 relaxation obtained from 3D FLASH MRI. *Magnetic Resonance in Medicine*, *60*(6), 1396–1407. https://doi.org/10.1002/mrm.21732

Hill, J., Inder, T., Neil, J., Dierker, D., Harwell, J., & Van Essen, D. (2010). Similar patterns of cortical expansion during human development and evolution. *Proceedings of the National Academy of Sciences of the United States of America*, *107*(29), 13135–13140. https://doi.org/10.1073/pnas.1001229107

Hillebrand, A., Tewarie, P., Van Dellen, E., Yu, M., Carbo, E. W. S., Douw, L., Gouw, A. A., Van Straaten, E. C. W., & Stam, C. J. (2016). Direction of information flow in large-scale resting-state networks is frequency-dependent. *Proceedings of the National Academy of Sciences of the United States of America*, *113*(14), 3867–3872. https://doi.org/10.1073/pnas.1515657113

Honey, C. J., Sporns, O., Cammoun, L., Gigandet, X., Thiran, J. P., Meuli, R., & Hagmann, P. (2009). Predicting human resting-state functional connectivity from structural connectivity. *Proceedings of the National Academy of Sciences of the United States of America*, *106*(6), 2035–2040. https://doi.org/10.1073/pnas.0811168106

Hoopes, A., Mora, J. S., Dalca, A. V., Fischl, B., & Hoffmann, M. (2022). SynthStrip: skull-stripping for any brain image. *NeuroImage*, *260*(June), 119474. https://doi.org/10.1016/j.neuroimage.2022.119474

Hunt, B. A. E., Tewarie, P. K., Mougin, O. E., Geades, N., Jones, D. K., Singh, K. D., Morris, P. G., Gowland, P. A., & Brookes, M. J. (2016).

Relationships between cortical myeloarchitecture and electrophysiological networks. *Proceedings of the National Academy of Sciences of the United States of America*, *113*(47), 13510–13515. https://doi.org/10.1073/pnas.1608587113

Huntenburg, J. M., Bazin, P. L., Goulas, A., Tardif, C. L., Villringer, A., & Margulies, D. S. (2017). A Systematic Relationship Between Functional Connectivity and Intracortical Myelin in the Human Cerebral Cortex. *Cerebral Cortex*, *27*(2), 981–997. https://doi.org/10.1093/cercor/bhx030

Huntenburg, J. M., Bazin, P. L., & Margulies, D. S. (2018). Large-Scale Gradients in Human Cortical Organization. *Trends in Cognitive Sciences*, *22*(1), 21–31. https://doi.org/10.1016/j.tics.2017.11.002

Huxley, A. F., & Stämpfli, R. (1949). Evidence for saltatory conduction in peripheral myelinated nerve fibres. *The Journal of Physiology*, *108*(3), 315–339. http://www.ncbi.nlm.nih.gov/pubmed/16991863

Ibañez, S., Sengupta, N., Luebke, J. I., Wimmer, K., & Weaver, C. M. (2023). Myelin dystrophy impairs signal transmission and working memory in a multiscale model of the aging prefrontal cortex. *ELife*, *12*, 1–29. https://doi.org/10.7554/eLife.90964

Jenkinson, M., Beckmann, C. F., Behrens, T. E. J., Woolrich, M. W., & Smith, S. M. (2012). FSL. *NeuroImage*, *62*(2), 782–790. https://doi.org/10.1016/j.neuroimage.2011.09.015

Jeurissen, B., Tournier, J. D., Dhollander, T., Connelly, A., & Sijbers, J. (2014). Multi-tissue constrained spherical deconvolution for improved analysis of multi-shell diffusion MRI data. *NeuroImage*, *103*, 411–426. https://doi.org/10.1016/j.neuroimage.2014.07.061

Karimian, M., Dibenedetto, D., Moerel, M., Burwick, T., Westra, R. L., De Weerd, P., & Senden, M. (2019). Effects of synaptic and myelin plasticity on learning in a network of Kuramoto phase oscillators. *Chaos*, *29*(8). https://doi.org/10.1063/1.5092786

Koch, M. A., Norris, D. G., & Hund-Georgiadis, M. (2002). An investigation of functional and anatomical connectivity using magnetic resonance imaging. *NeuroImage*, *16*(1), 241–250. https://doi.org/10.1006/nimg.2001.1052

Kong, R., Yang, Q., Gordon, E., Xue, A., Yan, X., Orban, C., Zuo, X. N., Spreng, N., Ge, T., Holmes, A., Eickhoff, S., & Yeo, B. T. T. (2021). Individual-Specific Areal-Level Parcellations Improve Functional Connectivity Prediction of Behavior. *Cerebral Cortex*, *31*(10), 4477–4500. https://doi.org/10.1093/cercor/bhab101

Lee, H., Novikov, D. S., & Fieremans, E. (2021). *Removal of Partial Fourier-Induced Gibbs (RPG) Ringing artifacts in MRI*. *November 2020*, 3–7. https://doi.org/10.1002/mrm.28830

Lee, Y., Morrison, B. M., Li, Y., Lengacher, S., Farah, M. H., Hoffman, P. N., Liu, Y., Tsingalia, A., Jin, L., Zhang, P. W., Pellerin, L., Magistretti, P. J., & Rothstein, J. D. (2012). Oligodendroglia metabolically support axons and contribute to neurodegeneration. *Nature*, *487*(7408), 443–448. https://doi.org/10.1038/nature11314

Lillie, R. S. (1925). FACTORS AFFECTING TRANSMISSION AND RECOVERY IN THE PASSIVE IRON NERVE MODEL. *Journal of General Physiology*, *7*(4), 473–507. https://doi.org/10.1085/jgp.7.4.473

Litwińczuk, M. C., Muhlert, N., Cloutman, L., Trujillo-Barreto, N., & Woollams, A. (2022). Combination of structural and functional connectivity explains unique variation in specific domains of cognitive function. *NeuroImage*, *262*(February), 119531. https://doi.org/10.1016/j.neuroimage.2022.119531

Liu, Z. Q., Shafiei, G., Baillet, S., & Misic, B. (2023). Spatially heterogeneous structure-function coupling in haemodynamic and electromagnetic brain networks. *NeuroImage*, *278*(July), 120276. https://doi.org/10.1016/j.neuroimage.2023.120276

Lord, L. D., Expert, P., Huckins, J. F., & Turkheimer, F. E. (2013). Cerebral energy metabolism and the brain's functional network architecture:

An integrative review. *Journal of Cerebral Blood Flow and Metabolism*, *33*(9), 1347–1354. https://doi.org/10.1038/jcbfm.2013.94

Lu, W. Da, Nelson, M. C., Leppert, I. R., Campbell, J. S. W., Schiavi, S., Pike, G. B., Rowley, C. D., Daducci, A., & Tardif, C. L. (2025). Mapping the aggregate g-ratio of white matter tracts using multi-modal MRI. *Imaging Neuroscience*. https://doi.org/10.1162/IMAG.a.49

Mahjoory, K., Schoffelen, J. M., Keitel, A., & Gross, J. (2020). The frequency gradient of human resting-state brain oscillations follows cortical hierarchies. *ELife*, *9*, 1–18. https://doi.org/10.7554/ELIFE.53715

Maier-Hein, K. H., Neher, P. F., Houde, J. C., Côté, M. A., Garyfallidis, E., Zhong, J., Chamberland, M., Yeh, F. C., Lin, Y. C., Ji, Q., Reddick, W. E., Glass, J. O., Chen, D. Q., Feng, Y., Gao, C., Wu, Y., Ma, J., Renjie, H., Li, Q., … Descoteaux, M. (2017). The challenge of mapping the human connectome based on diffusion tractography. *Nature Communications*, *8*(1). https://doi.org/10.1038/s41467-017-01285-x

Mancini, M., Giulietti, G., Dowell, N., Spanò, B., Harrison, N., Bozzali, M., & Cercignani, M. (2018). Introducing axonal myelination in connectomics: A preliminary analysis of g-ratio distribution in healthy subjects. *NeuroImage*, *182*, 351–359. https://doi.org/10.1016/j.neuroimage.2017.09.018

Mancini, M., Tian, Q., Fan, Q., Cercignani, M., & Huang, S. Y. (2021). Dissecting whole-brain conduction delays through MRI microstructural measures. *Brain Structure and Function*, *226*(8), 2651–2663. https://doi.org/10.1007/s00429-021-02358-w

Margulies, D. S., Ghosh, S. S., Goulas, A., Falkiewicz, M., Huntenburg, J. M., Langs, G., Bezgin, G., Eickhoff, S. B., Castellanos, F. X., Petrides, M., Jefferies, E., & Smallwood, J. (2016). Situating the default-mode network along a principal gradient of macroscale cortical organization. *Proceedings of the National Academy of Sciences of the United States of America*, *113*(44), 12574–12579. https://doi.org/10.1073/pnas.1608282113

Marques, J. P., Kober, T., Krueger, G., van der Zwaag, W., Van de Moortele, P. F., & Gruetter, R. (2010). MP2RAGE, a self bias-field corrected sequence for improved segmentation and T1-mapping at high field. *NeuroImage*, *49*(2), 1271–1281. https://doi.org/10.1016/j.neuroimage.2009.10.002

Messaritaki, E., Foley, S., Schiavi, S., Magazzini, L., Routley, B., Jones, D. K., & Singh, K. D. (2021). Predicting meg resting-state functional connectivity from microstructural information. *Network Neuroscience*, *5*(2), 477–504. https://doi.org/10.1162/netn_a_00187

Mesulam, M. M. (1998). From sensation to cognition. *Brain*, *121*(6), 1013–1052. https://doi.org/10.1093/brain/121.6.1013

Metzler-Baddeley, C., Foley, S., de Santis, S., Charron, C., Hampshire, A., Caeyenberghs, K., & Jones, D. K. (2017). Dynamics of White Matter Plasticity Underlying Working Memory Training: Multimodal Evidence from Diffusion MRI and Relaxometry. *Journal of Cognitive Neuroscience*, *29*(9), 1509–1520. https://doi.org/10.1162/jocn_a_01127

Mori, S., & Barker, P. B. (1999). Diffusion magnetic resonance imaging: Its principle and applications. *The Anatomical Record*, *257*(3), 102–109. https://doi.org/10.1002/(SICI)1097-0185(19990615)257:3<102::AID-AR7>3.0.CO;2-6

Mori, S., & Van Zijl, P. C. M. (2002). Fiber tracking: Principles and strategies - A technical review. *NMR in Biomedicine*, *15*(7–8), 468–480. https://doi.org/10.1002/nbm.781

Mount, C. W., & Monje, M. (2017). Wrapped to Adapt: Experience-Dependent Myelination. *Neuron*, *95*(4), 743–756. https://doi.org/10.1016/j.neuron.2017.07.009

Murray, J. D., Bernacchia, A., Freedman, D. J., Romo, R., Wallis, J. D., Cai, X., Padoa-Schioppa, C., Pasternak, T., Seo, H., Lee, D., & Wang, X. J. (2014). A hierarchy of intrinsic timescales across primate cortex. *Nature Neuroscience*, *17*(12), 1661–1663.

https://doi.org/10.1038/nn.3862

Mussard, E., Hilbert, T., Forman, C., Meuli, R., Thiran, J. P., & Kober, T. (2020). Accelerated MP2RAGE imaging using Cartesian phyllotaxis readout and compressed sensing reconstruction. *Magnetic Resonance in Medicine*, *84*(4), 1881–1894. https://doi.org/10.1002/mrm.28244

Narine, M., & Colognato, H. (2022). Current Insights Into Oligodendrocyte Metabolism and Its Power to Sculpt the Myelin Landscape. *Frontiers in Cellular Neuroscience*, *16*(April), 1–17. https://doi.org/10.3389/fncel.2022.892968

Nave, K. A. (2010). Myelination and the trophic support of long axons. *Nature Reviews Neuroscience*, *11*(4), 275–283. https://doi.org/10.1038/nrn2797

Nave, K. A., Asadollahi, E., & Sasmita, A. (2023). Expanding the function of oligodendrocytes to brain energy metabolism. *Current Opinion in Neurobiology*, *83*, 102782. https://doi.org/10.1016/j.conb.2023.102782

Nave, K. A., & Werner, H. B. (2014). Myelination of the nervous system: Mechanisms and functions. *Annual Review of Cell and Developmental Biology*, *30*, 503–533. https://doi.org/10.1146/annurev-cellbio-100913-013101

Nelson, M. C., Royer, J., da Lu, W., Leppert, I. R., Campbell, J. S. W., Schiavi, S., Jin, H., Tavakol, S., Vos de Wael, R., Rodriguez-Cruces, R., Pike, G. B., Bernhardt, B. C., Daducci, A., Misic, B., & Tardif, C. L. (2023). The human brain connectome weighted by the myelin content and total intra-axonal cross-sectional area of white matter tracts. *Network Neuroscience*, *7*(4), 1363–1388. https://doi.org/10.1162/netn_a_00330

Newman, M. (2010). Networks. In *Journal of Chemical Information and Modeling* (Vol. 53, Issue 9). Oxford University Press. https://doi.org/10.1093/acprof:oso/9780199206650.001.0001

Newman, M. E. J. (2003). The structure and function of complex networks. *SIAM Review*, *45*(2), 167–256. https://doi.org/10.1137/S003614450342480

Noori, R., Park, D., Griffiths, J. D., Bells, S., Frankland, P. W., Mabbott, D., & Lefebvre, J. (2020). Activity-dependent myelination: A glial mechanism of oscillatory self-organization in large-scale brain networks. *Proceedings of the National Academy of Sciences of the United States of America*, *117*(24), 13227–13237. https://doi.org/10.1073/pnas.1916646117

Nunez, P. L., & Srinivasan, R. (2014). Neocortical dynamics due to axon propagation delays in cortico-cortical fibers: EEG traveling and standing waves with implications for top-down influences on local networks and white matter disease. *Brain Research*, *1542*, 138–166. https://doi.org/10.1016/j.brainres.2013.10.036

Nunez, P. L., Srinivasan, R., & Fields, R. D. (2015). EEG functional connectivity, axon delays and white matter disease. *Clinical Neurophysiology*, *126*(1), 110–120. https://doi.org/10.1016/j.clinph.2014.04.003

Osmanlıoğlu, Y., Tunç, B., Parker, D., Elliott, M. A., Baum, G. L., Ciric, R., Satterthwaite, T. D., Gur, R. E., Gur, R. C., & Verma, R. (2019). System-level matching of structural and functional connectomes in the human brain. *NeuroImage*, *199*(May), 93–104. https://doi.org/10.1016/j.neuroimage.2019.05.064

Pajevic, S., Basser, P. J., & Fields, R. D. (2014). Role of myelin plasticity in oscillations and synchrony of neuronal activity. *Neuroscience*, *276*, 135–147. https://doi.org/10.1016/j.neuroscience.2013.11.007

Paquola, C., Vos De Wael, R., Wagstyl, K., Bethlehem, R. A. I., Hong, S. J., Seidlitz, J., Bullmore, E. T., Evans, A. C., Misic, B., Margulies, D. S., Smallwood, J., & Bernhardt, B. C. (2019). Microstructural and functional gradients are increasingly dissociated in transmodal cortices. *PLoS Biology*, *17*(5), 1–28. https://doi.org/10.1371/journal.pbio.3000284

Park, S. H., & Lefebvre, J. (2020). Synchronization and resilience in the Kuramoto white matter network model with adaptive state-dependent delays. *Journal of Mathematical Neuroscience*, *10*(1). https://doi.org/10.1186/s13408-020-00091-y

Patenaude, B., Smith, S. M., Kennedy, D. N., & Jenkinson, M. (2011). A Bayesian model of shape and appearance for subcortical brain segmentation. *NeuroImage*, *56*(3), 907–922. https://doi.org/10.1016/j.neuroimage.2011.02.046

Petkoski, S., Ritter, P., & Jirsa, V. K. (2023). White-matter degradation and dynamical compensation support age-related functional alterations in human brain. *Cerebral Cortex*, *33*(10), 6241–6256. https://doi.org/10.1093/cercor/bhac500

Popp, J. L., Thiele, J. A., Faskowitz, J., Seguin, C., Sporns, O., & Hilger, K. (2024). Structural-functional brain network coupling predicts human cognitive ability. *NeuroImage*, *290*(October 2023), 120563. https://doi.org/10.1016/j.neuroimage.2024.120563

Preti, M. G., & Van De Ville, D. (2019). Decoupling of brain function from structure reveals regional behavioral specialization in humans. *Nature Communications*, *10*(1), 1–7. https://doi.org/10.1038/s41467-019-12765-7

Ramos-Cabrer, P., Cabrera-Zubizarreta, A., Padro, D., Matute-González, M., Rodríguez-Antigüedad, A., & Matute, C. (2025). Reversible reduction in brain myelin content upon marathon running. *Nature Metabolism*, *7*(April). https://doi.org/10.1038/s42255-025-01244-7

Roberts, J. A., Perry, A., Roberts, G., Mitchell, P. B., & Breakspear, M. (2017). Consistency-based thresholding of the human connectome. *NeuroImage*, *145*(September 2016), 118–129. https://doi.org/10.1016/j.neuroimage.2016.09.053

Rowley, C. D., Campbell, J. S. W., Wu, Z., Leppert, I. R., Rudko, D. A., Pike, G. B., & Tardif, C. L. (2021). A model-based framework for correcting B1+ inhomogeneity effects in magnetization transfer saturation and inhomogeneous magnetization transfer saturation maps. *Magnetic Resonance in Medicine*, *86*(4), 2192–2207. https://doi.org/10.1002/mrm.28831

Royer, J., Rodríguez-Cruces, R., Tavakol, S., Larivière, S., Herholz, P., Li, Q., Vos de Wael, R., Paquola, C., Benkarim, O., Park, B., Lowe, A. J., Margulies, D., Smallwood, J., Bernasconi, A., Bernasconi, N., Frauscher, B., & Bernhardt, B. C. (2022). An Open MRI Dataset For Multiscale Neuroscience. *Scientific Data*, *9*(1), 569. https://doi.org/10.1038/s41597-022-01682-y

Saab, A. S., Tzvetavona, I. D., Trevisiol, A., Baltan, S., Dibaj, P., Kusch, K., Möbius, W., Goetze, B., Jahn, H. M., Huang, W., Steffens, H., Schomburg, E. D., Pérez-Samartín, A., Pérez-Cerdá, F., Bakhtiari, D., Matute, C., Löwel, S., Griesinger, C., Hirrlinger, J., … Nave, K. A. (2016). Oligodendroglial NMDA Receptors Regulate Glucose Import and Axonal Energy Metabolism. *Neuron*, *91*(1), 119–132. https://doi.org/10.1016/j.neuron.2016.05.016

Salvador, R., Suckling, J., Coleman, M. R., Pickard, J. D., Menon, D., & Bullmore, E. (2005). Neurophysiological architecture of functional magnetic resonance images of human brain. *Cerebral Cortex*, *15*(9), 1332–2342. https://doi.org/10.1093/cercor/bhi016

Saskia Hübner, N., Mechling, A. E., Lee, H. L., Reisert, M., Bienert, T., Hennig, J., von Elverfeldt, D., & Harsan, L. A. (2017). The connectomics of brain demyelination: Functional and structural patterns in the cuprizone mouse model. *NeuroImage*, *146*(February 2016), 1–18. https://doi.org/10.1016/j.neuroimage.2016.11.008

Schaefer, A., Kong, R., Gordon, E. M., Laumann, T. O., Zuo, X.-N., Holmes, A. J., Eickhoff, S. B., & Yeo, B. T. T. (2018). Local-Global Parcellation of the Human Cerebral Cortex from Intrinsic Functional Connectivity MRI. *Cerebral Cortex*, *28*(9), 3095–3114. https://doi.org/10.1093/cercor/bhx179

Scheeringa, R., & Fries, P. (2019). Cortical layers, rhythms and BOLD signals. *NeuroImage*, *197*(November 2017), 689–698. https://doi.org/10.1016/j.neuroimage.2017.11.002

Schiavi, S., Lu, P., Weigel, M., Lutti, A., Jones, D. K., Kappos, L., Granziera, C., & Daducci, A. (2022). Bundle Myelin Fraction (BMF)

Mapping of Different White Matter Connections Using Microstructure Informed Tractography. *NeuroImage*, 118922. https://doi.org/10.1016/j.neuroimage.2022.118922

Schilling, K. G., Daducci, A., Maier-Hein, K., Poupon, C., Houde, J. C., Nath, V., Anderson, A. W., Landman, B. A., & Descoteaux, M. (2019). Challenges in diffusion MRI tractography – Lessons learned from international benchmark competitions. *Magnetic Resonance Imaging*, *57*(November 2018), 194–209. https://doi.org/10.1016/j.mri.2018.11.014

Seguin, C., Sporns, O., & Zalesky, A. (2023). Brain network communication: concepts, models and applications. *Nature Reviews Neuroscience*, *24*(9), 557–574. https://doi.org/10.1038/s41583-023-00718-5

Seguin, C., Tian, Y., & Zalesky, A. (2020). Network communication models improve the behavioral and functional predictive utility of the human structural connectome. *Network Neuroscience*, *4*(4), 980–1006. https://doi.org/10.1162/netn_a_00161

Sepulcre, J., Liu, H., Talukdar, T., Martincorena, I., Thomas Yeo, B. T., & Buckner, R. L. (2010). The organization of local and distant functional connectivity in the human brain. *PLoS Computational Biology*, *6*(6), 1–15. https://doi.org/10.1371/journal.pcbi.1000808

Shafiei, G., Baillet, S., & Misic, B. (2022). Human electromagnetic and haemodynamic networks systematically converge in unimodal cortex and diverge in transmodal cortex. *PLoS Biology*, *20*(8), 1–27. https://doi.org/10.1371/journal.pbio.3001735

Shine, J. M., Breakspear, M., Bell, P. T., Ehgoetz Martens, K., Shine, R., Koyejo, O., Sporns, O., & Poldrack, R. A. (2019). Human cognition involves the dynamic integration of neural activity and neuromodulatory systems. *Nature Neuroscience*, *22*(2), 289–296. https://doi.org/10.1038/s41593-018-0312-0

Slater, D. A., Melie-Garcia, L., Preisig, M., Kherif, F., Lutti, A., & Draganski, B. (2019). Evolution of white matter tract microstructure across the life span. *Human Brain Mapping*, *40*(7), 2252–2268. https://doi.org/10.1002/hbm.24522

Smith, R. E., Tournier, J. D., Calamante, F., & Connelly, A. (2012). Anatomically-constrained tractography: Improved diffusion MRI streamlines tractography through effective use of anatomical information. *NeuroImage*, *62*(3), 1924–1938. https://doi.org/10.1016/j.neuroimage.2012.06.005

Smith, R. E., Tournier, J. D., Calamante, F., & Connelly, A. (2015). SIFT2: Enabling dense quantitative assessment of brain white matter connectivity using streamlines tractography. *NeuroImage*, *119*, 338–351. https://doi.org/10.1016/j.neuroimage.2015.06.092

Smith, S. M. (2002). Fast robust automated brain extraction. *Human Brain Mapping*, *17*(3), 143–155. https://doi.org/10.1002/hbm.10062

Smith, S. M., Jenkinson, M., Woolrich, M. W., Beckmann, C. F., Behrens, T. E. J., Johansen-Berg, H., Bannister, P. R., De Luca, M., Drobnjak, I., Flitney, D. E., Niazy, R. K., Saunders, J., Vickers, J., Zhang, Y., De Stefano, N., Brady, J. M., & Matthews, P. M. (2004). Advances in functional and structural MR image analysis and implementation as FSL. *NeuroImage*, *23*(SUPPL. 1), 208–219. https://doi.org/10.1016/j.neuroimage.2004.07.051

Sporns, O. (2010). Networks of the Brain. In *Networks of the Brain*. The MIT Press. https://doi.org/10.7551/mitpress/8476.001.0001

Sporns, O. (2011). The human connectome: A complex network. *Annals of the New York Academy of Sciences*, *1224*(1), 109–125. https://doi.org/10.1111/j.1749-6632.2010.05888.x

Sporns, O. (2013). Structure and function of complex brain networks. *Dialogues Clin Neurosci.*, 247–262.

Stikov, N., Campbell, J. S. W., Stroh, T., Lavelée, M., Frey, S., Novek, J., Nuara, S., Ho, M. K., Bedell, B. J., Dougherty, R. F., Leppert, I. R., Boudreau, M., Narayanan, S., Duval, T., Cohen-Adad, J., Picard, P. A., Gasecka, A., Côté, D., & Pike, G. B. (2015). In vivo histology of the myelin g-ratio with magnetic resonance imaging. *NeuroImage*, *118*, 397–405. https://doi.org/10.1016/j.neuroimage.2015.05.023

Suárez, L. E., Markello, R. D., Betzel, R. F., & Misic, B. (2020). Linking Structure and Function in Macroscale Brain Networks. *Trends in Cognitive Sciences*. https://doi.org/10.1016/j.tics.2020.01.008

Sydnor, V. J., Larsen, B., Bassett, D. S., Alexander-Bloch, A., Fair, D. A., Liston, C., Mackey, A. P., Milham, M. P., Pines, A., Roalf, D. R., Seidlitz, J., Xu, T., Raznahan, A., & Satterthwaite, T. D. (2021). Neurodevelopment of the association cortices: Patterns, mechanisms, and implications for psychopathology. *Neuron*, *109*(18), 2820–2846. https://doi.org/10.1016/j.neuron.2021.06.016

Talidou, A., & Lefebvre, J. (2025). Spatial Heterogeneity in Myelin Sheathing Impacts Signaling Reliability and Susceptibility to Injury. *ENeuro*, *12*(2), 1–18. https://doi.org/10.1523/ENEURO.0402-24.2025

Tasaki, I. (1939). THE ELECTRO-SALTATORY TRANSMISSION OF THE NERVE IMPULSE AND THE EFFECT OF NARCOSIS UPON THE NERVE FIBER. *American Journal of Physiology*, *127*(2), 211–227. https://doi.org/10.1152/ajplegacy.1939.127.2.211

Tewarie, P., Bright, M. G., Hillebrand, A., Robson, S. E., Gascoyne, L. E., Morris, P. G., Meier, J., Van Mieghem, P., & Brookes, M. J. (2016). Predicting haemodynamic networks using electrophysiology: The role of non-linear and cross-frequency interactions. *NeuroImage*, *130*, 273–292. https://doi.org/10.1016/j.neuroimage.2016.01.053

Thomas Yeo, B. T., Krienen, F. M., Sepulcre, J., Sabuncu, M. R., Lashkari, D., Hollinshead, M., Roffman, J. L., Smoller, J. W., Zöllei, L., Polimeni, J. R., Fisch, B., Liu, H., & Buckner, R. L. (2011). The organization of the human cerebral cortex estimated by intrinsic functional connectivity. *Journal of Neurophysiology*, *106*(3), 1125–1165. https://doi.org/10.1152/jn.00338.2011

Tournier, J.-D., Calamante, F., & Connelly, A. (2010). Improved probabilistic streamlines tractography by 2 nd order integration over fibre orientation distributions. *Ismrm*, *88*(2003), 2010. https://cds.ismrm.org/protected/10MProceedings/PDFfiles/1670_4298.pdf

Tournier, J. D., Calamante, F., & Connelly, A. (2012). MRtrix: Diffusion tractography in crossing fiber regions. *International Journal of Imaging Systems and Technology*, *22*(1), 53–66. https://doi.org/10.1002/ima.22005

Tournier, J. D., Smith, R., Raffelt, D., Tabbara, R., Dhollander, T., Pietsch, M., Christiaens, D., Jeurissen, B., Yeh, C. H., & Connelly, A. (2019). MRtrix3: A fast, flexible and open software framework for medical image processing and visualisation. *NeuroImage*, *202*. https://doi.org/10.1016/j.neuroimage.2019.116137

Trevisiol, A., Saab, A. S., Winkler, U., Marx, G., Imamura, H., Möbius, W., Kusch, K., Nave, K. A., & Hirrlinger, J. (2017). Monitoring ATP dynamics in electrically active white matter tracts. *ELife*, *6*, 1–17. https://doi.org/10.7554/eLife.24241

Tustison, N. J., Avants, B. B., Cook, P. A., Zheng, Y., Egan, A., Yushkevich, P. A., & Gee, J. C. (2010). N4ITK: Improved N3 bias correction. *IEEE Transactions on Medical Imaging*, *29*(6), 1310–1320. https://doi.org/10.1109/TMI.2010.2046908

van den Heuvel, M. P., Mandl, R. C. W., Stam, C. J., Kahn, R. S., & Hulshoff Pol, H. E. (2010). Aberrant Frontal and Temporal Complex Network Structure in Schizophrenia: A Graph Theoretical Analysis. *Journal of Neuroscience*, *30*(47), 15915–15926. https://doi.org/10.1523/JNEUROSCI.2874-10.2010

van den Heuvel, Martijn P., & Sporns, O. (2013). Network hubs in the human brain. *Trends in Cognitive Sciences*, *17*(12), 683–696. https://doi.org/10.1016/j.tics.2013.09.012

Van Essen, D. C., Smith, S. M., Barch, D. M., Behrens, T. E. J., Yacoub, E., & Ugurbil, K. (2013). The WU-Minn Human Connectome Project: An overview. *NeuroImage*, *80*, 62–79. https://doi.org/10.1016/j.neuroimage.2013.05.041

Vázquez-Rodríguez, B., Suárez, L. E., Markello, R. D., Shafiei, G., Paquola, C., Hagmann, P., Van Den Heuvel, M. P., Bernhardt, B. C., Spreng, R. N., & Misic, B. (2019). Gradients of structure–function tethering across neocortex. *Proceedings of the National Academy of Sciences of*

the United States of America, *116*(42), 21219–21227. https://doi.org/10.1073/pnas.1903403116

Veraart, J., Fieremans, E., & Novikov, D. S. (2016). Diffusion MRI noise mapping using random matrix theory. *Magnetic Resonance in Medicine*, *76*(5), 1582–1593. https://doi.org/10.1002/mrm.26059

Veraart, J., Novikov, D. S., Christiaens, D., Ades-aron, B., Sijbers, J., & Fieremans, E. (2016). Denoising of diffusion MRI using random matrix theory. *NeuroImage*, *142*, 394–406. https://doi.org/10.1016/j.neuroimage.2016.08.016

Von Stein, A., Chiang, C., & König, P. (2000). Top-down processing mediated by interareal synchronization. *Proceedings of the National Academy of Sciences of the United States of America*, *97*(26), 14748–14753. https://doi.org/10.1073/pnas.97.26.14748

Wang, P., Kong, R., Kong, X., Liégeois, R., Orban, C., Deco, G., van den Heuvel, M. P., & Thomas Yeo, B. T. (2019). Inversion of a large-scale circuit model reveals a cortical hierarchy in the dynamic resting human brain. *Science Advances*, *5*(1). https://doi.org/10.1126/sciadv.aat7854

Woolrich, M. W., Jbabdi, S., Patenaude, B., Chappell, M., Makni, S., Behrens, T., Beckmann, C., Jenkinson, M., & Smith, S. M. (2009). Bayesian analysis of neuroimaging data in FSL. *NeuroImage*, *45*(1 Suppl), S173–S186. https://doi.org/10.1016/j.neuroimage.2008.10.055

Yeatman, J. D., Wandell, B. A., & Mezer, A. A. (2014). Lifespan maturation and degeneration of human brain white matter. *Nature Communications*, *5*. https://doi.org/10.1038/ncomms5932

Zamani Esfahlani, F., Faskowitz, J., Slack, J., Mišić, B., & Betzel, R. F. (2022). Local structure-function relationships in human brain networks across the lifespan. *Nature Communications*, *13*(1). https://doi.org/10.1038/s41467-022-29770-y

Zatorre, R. J., Fields, R. D., & Johansen-Berg, H. (2012). Plasticity in gray and white: Neuroimaging changes in brain structure during learning. *Nature Neuroscience*, *15*(4), 528–536. https://doi.org/10.1038/nn.3045

Zhang, Y., Brady, M., & Smith, S. (2001). Segmentation of brain MR images through a hidden Markov random field model and the expectation-maximization algorithm. *IEEE Transactions on Medical Imaging*, *20*(1), 45–57. https://doi.org/10.1109/42.906424

Acknowledgments

The authors acknowledge research support from the National Science and Engineering Research Council of Canada (NSERC), the Canadian Institutes for Health Research (CIHR), Fonds de recherche du Québec – Santé (FRQ-S), CFREF Healthy Brains for Healthy Lives, the Killam Trusts, and Brain Canada.

Competing interests

The authors declare no competing interests.